# DEVELOPMENT OF MECHANICALLY ROBUST WATER-REPELLENT SURFACES

BY

**ABUDULIKEN BAKE**

A Thesis Presented to the
DEANSHIP OF GRADUATE STUDIES

**KING FAHD UNIVERSITY OF PETROLEUM & MINERALS**

DHAHRAN, SAUDI ARABIA

In Partial Fulfillment of the
Requirements for the Degree of

**MASTER OF SCIENCE**

**In**

**MATERIAL SCIENCE AND ENGINEERING**

**JANUARY 2017**

KING FAHD UNIVERSITY OF PETROLEUM & MINERALS
DHAHRAN- 31261, SAUDI ARABIA
**DEANSHIP OF GRADUATE STUDIES**

This thesis, written by **ABUDULIKEN BAKE** under the direction his thesis advisor and approved by his thesis committee, has been presented and accepted by the Dean of Graduate Studies, in partial fulfillment of the requirements for the degree of **MASTER OF SCIENCE IN MATERIALS SCIENCE & ENGINEERING.**

Merah

Dr. Neçar Merah
(Advisor)

Dr. Zuhair Gasem
Department Chairman

Dr. A. Gondal

Dr. Mohammed Ashraf Gondal
(Member)

Dr. Salam A. Zummo
Dean of Graduate Studies

Dr. Numan Abu-Dheir
(Member)

23/2/17

Date

I dedicate this thesis work to my whole family members who always encourage me and give me intrinsic motivation to pursue my academic goal.

# ACKNOWLEDGMENTS

بِسْمِ اللَّهِ الرَّحْمَنِ الرَّحِيم

All praises are due to Allah who gave me knowledge, wisdom and strength to successfully complete my Master degree in KFUPM, KSA.

I would like to thank my very gentle and kind advisor Prof. Neçar Merah for his generous support, guidance and encouragement all along the way. My sincere appreciation goes to him for sharing his knowledge, showing me enough patience.

I would like to thank my thesis committee members prof. M. A. Gondal and Dr. Numan Abu-Dheir for their support and kind help for successfully conduction of my experimental work. I greatly appreciate the skills what I learnt during working at Prof. Gondal' s lab.

I would also like to thank Dr. Asif Matin for his kind help, useful discussions and advises. The generous help of Mr. Talal Qahtan, Ph.D. student, working in Prof. Gondal' s lab is highly appreciated.

Last but not least, I really appreciate and thank to my beloved family members. My parents' support, understanding, endless prayers and their love are my intrinsic motivation to successfully complete my master study at KFUPM. Without my brothers and sisters' kind encouragement and support, it would be hard for me to achieve appreciable results from my thesis work.

# TABLE OF CONTENTS

# LIST OF TABLES

# LIST OF FIGURES

# LIST OF ABBREVIATIONS

**CA** : Contact Angle

**SA** : Sliding Angle

**AA** : Advancing Angle

**RA** : Receding Angle

**H** : Hysteresis

**MTMS** : Methyltrimethoxysilane

**PFOTS** : 1H,1H,2H,2H-Perfluorooctyl-trichlorosilane

**GLYMO** : (3-Glycidyloxypropyl)trimethoxysilane

**XPS** : X-ray Photoelectron Spectroscopy

# ABSTRACT

Full Name : [Abuduliken Bake]
Thesis Title : [Development of Mechanically Robust Water-Repellant Surfaces]
Major Field : [Material Science and Engineering]
Date of Degree : [January 2017]

Superhydrophobic surfaces have recently attracted a lot of attention due to their high water repellency along with a wide range of applications in many fields. The application of such surfaces for self-cleaning purposes, such as in solar cell modules, has been limited due to lack of mechanical robustness, thermal stability and ultraviolet radiation resistance. The fabrication of superhydrophobic surfaces with mechanical robustness and high transmittance of visible light is still a major challenge. This research presents a method for fabrication of transparent, robust and stable superhydrophobic surfaces by simple spray-coating process. In this work, proper spraying cycles and mixtures of silane and 1%wt $SiO_2$ nanoparticles has resulted in water contact angles as high as 170˚ with hysteresis of 6˚ and sliding angle of 1°. Developed surfaces during this work also exhibited excellent stability under pressurized jet water, abrasion and ultraviolet radiations. Improvement of visible light transmissivity was achieved by annealing the surface up to a temperature of 300°C. Measured optical transmissivity was found to be within 90% of that of virgin glass. With the unique combination of the above mentioned desired properties of the fabricated surface, this makes them promising candidate for outdoor self-cleaning applications even under harsh environmental conditions.

# ملخص الرسالة

**الاسم الكامل: عبد الحكيم باقي**

**عنوان الرسالة: تحضير اسطح طاردة للماء مستقرة مكيانيكا**

**التخصص: علم وهندسة المواد**

**تاريخ الدرجة العلمية: يناير 2017**

تلقى الطلاء الطارد للماء اهمية كبيرة نظرا لقابلية تطبيقه في عدة مجالات. يظل تطبيق هذا الطلاء لانتاج اسطح ذاتية التنظيف المستخدمة في مجال الخلايا الشمسية محدودا جدا نتيجة لنفاذيتة المنخفضة للطيف الشمسي المرئي ومتانتة المنخفضة لمقاومة الظروف القاسية.

تركز هذه الدراسة البحثية على انتاج اسطح طاردة للماء (ذاتية التنظيف) لها متانة عالية و نفاذية اعلى للطيف الشمسي المرئي باستخدام طريقة طلاء الرش. الطلاء يتكون من عدة طبقات من مادة الطلاء المستخدمة والتي هى عبارة عن مزيج من مركب غير عضوي ذو توتر سطحي منخفض مع ثاني اكسيد السليكون النانوي. الاسطح المطلية التي تم انتاجها خلال هذه الدراسة لها زاوية تلامس عالية تصل الى 170 درجة وزاوية ميلان مقدارها درجة واحدة. اضافة الى ذلك تتمتع باستقرارية عالية تحت اختبار رش المياة والكشط الميكانيكي والاشعاع فوق البنفسجي. اظهرت الاسطح المطلية نفاذية ضوئية عالية تصل الى 90 % من نفاذية الزجاج غير المطلي بعد تسخينها عند 300 درجة مئوية. بناء على ما تم ذكره، من الممكن استخدام نتائج هذه الدراسة لانتاج اسطح شفافة ذاتية التنظيف وتطبيقها في الميدان حتى تحت ظروف قاسية جدا.

# CHAPTER 1

# INTRODUCTION

## 1.1 Statement of the problem

Green and sustainable energy development is becoming a popular research area worldwide since this is the only way to reduce and tackle the environmental pollution problems. Solar energy conversion is considered as a major source of green energy and relevant devices such as photovoltaic (PV) systems can convert the solar radiation to electricity without compromising on the environment. Worldwide ongoing research on minimizing cost and improving efficiency of solar cells has led to the marketing of solar modules based on Si wafers having up to 25% solar conversion efficiency [1][2]. Therefore, maintaining this amount of conversion efficiency of solar cells is very crucial to make the PV systems a more attractive alternative energy source.

One of the main challenges for maintaining the energy conversion efficiency of solar cells is to keep the solar and photovoltaic (PV) panels as clean as possible. This is a daunting task in desert environments where the solar radiation is abundant and at the same time, dust accumulation is inevitable. Accumulation and deposition of the dust particles on the solar PV panel is a quite complicated process which is mainly governed by the weather conditions at the installation place. Dust deposition is mainly influenced by the characteristics of the dust particles, surfaces of the panels and environment. The dust particles and other particulates can lead to efficiency reduction in PV modules by certain percentage depending on the time duration and environment conditions. A research conducted by Salim et al. [3] found that PV system in a solar-village near Riyadh, Saudi Arabia end up with 32% reduction on efficiency after 8 months of soiling (dust accumulation) on the PV panels. A similar study conducted by Wakim [4] in Kuwait revealed reduction of 17% in efficiency after 6 days only. Sometimes because of the uncertainty of the desert environment, the actual reduction of efficiency may be much more significant within very short time. In areas where the rain occurs often, PV solar panels can recover part or most of lost efficiency [5].

A number of techniques have been developed by researchers worldwide to keep the surface out of mud, dust and contaminations, minimize dust settlement on PV panel surfaces to facilitate the harvesting of solar energy by solar cell materials. These techniques included cleaning the surface by high-pressure water fluids, mechanical methods (such as cleaning with mechanical robotic brushes and vibration), electrostatic removal of dusts and fabricating surfaces with self-cleaning properties [6]–[9] as shown in Figure 1 . Self-cleaning surface do not require intensive labor work and/or consume huge amounts of water and energy, thus save time, money and water.

Figure 1 Various ways of cleaning the solar PV panel surfaces.

## 1.2 Water-repellent self-cleaning surfaces

Modifying the surface to make it superhydrophobic with self-cleaning properties is a very attractive option to maintain or recover the efficiency of solar PV panels. Due to their extremely water-repellant nature, water droplets roll off superhydrophobic surface at a very small tilting angle or even without tilting, collecting dust and dirt particles, and leaving behind a clean and unwet surface. Hence, the development of superhydrophobic surfaces has been the focus of many studies for various ranges of applications, such as self-cleaning surface for the photovoltaic (PV) panels, frictionless transport of water through pipes with less energy consumptions [10].

The last decade or two has seen a significant surge in the number of publications related to the fabrication of superhydrophobic surfaces. Researchers have been successful in combining several desirable characteristics such as self-cleaning, optical transparency, etc. in one product [11]–[16].

## 1.3 Challenges of self-cleaning surfaces

In addition to water-repellency and the self-cleaning effect, there are also some other important properties of the coatings that researchers need to consider as well, such as high transmittance of visible light or antireflection index. Usually, the surface chemistry and surface roughness govern the surface hydrophobicity; low surface energy chemistry with optimum surface roughness result in superhydrophobic nature. However, if the fabricated surface intended application is for the solar energy harvesting applications, such as PV panel cover, the transmittance of the surface shouldn’t be compromised so that solar cell material harvesting the sunlight radiation will not be affected. Since the surface roughness and the transmittance are two contradictory concepts with the increase in roughness resulting in the decrease in transmittance, therefore a balance between the surface roughness and transmittance should be tuned properly. Mechanical stability/robustness and Ultraviolet (UV) long term radiation resistance of the fabricated superhydrophobic surface is also crucial for solar cell applications. The hierarchical rough micro/nano-structures of superhydrophobic coatings usually become distorted by abrasion and impact of dust particles can lead to detachment of the hydrophobic coating layer which consequently reduces the surface water repelling properties [17].

## 1.4 Scope of the work

Among the different techniques for the fabrication of water-repellant surfaces, the sol-gel route stands out due to its ease of processing, versatility and ability to fine tune surface characteristics.

In the present study, we will focus on the fabrication of water-repellent surfaces with self-cleaning ability by the deposition of specially prepared silane films using sol-gel technique. Special attention will be given to the ability of the surface to transmit light and to the mechanical robustness of the developed surfaces. The fabricated coatings are expected to resist UV radiation, abrasion and wear/tear during field applications.

# CHAPTER 2

# LITERATURE REVIEW

## 2.1 Water contact angle

Water contact angle measurement is a method that can be used for qualitatively determination of the surface free energy of the substances. Water contact angle refers to the angle formed by the intersection of the liquid-solid interface and the liquid-vapor interface as illustrated in the Figure 2 which is α. Water contact angle less than 90° means surface is hydrophilic and it has higher wettability, if higher than 90° means surface is hydrophobic and it has less wettability, superhydrophobic surface usually refers to that the water contact angle higher than 150°.

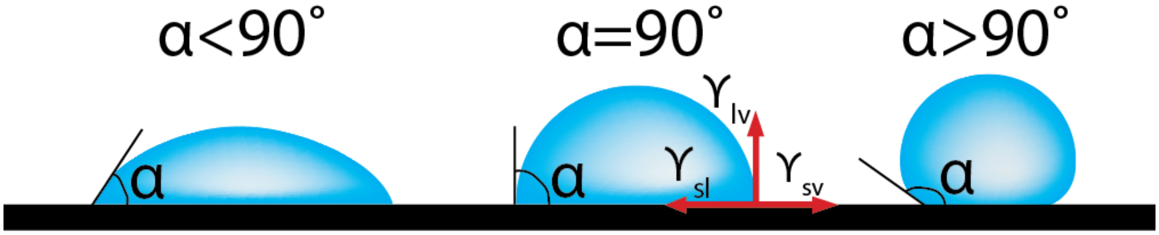

Figure 2 Illustration of water contact angle formed on the smooth solid surface

Water contact angle measurement can be easily conducted using the goniometer. In actual applications, measurement of static contact angle alone to characterize wetting behavior is not enough. During the motion of the liquid droplet, contact angle α formed as in the Figure 3 is called dynamic contact angle. Basically, the contact angles formed by expanding and contracting the liquid droplet [18] or by the motion of the liquid droplet is referred to as the advancing contact angle $\alpha_a$ and the receding contact angle $\alpha_r$, respectively, schematic illustration is showed in Figure 3 below.

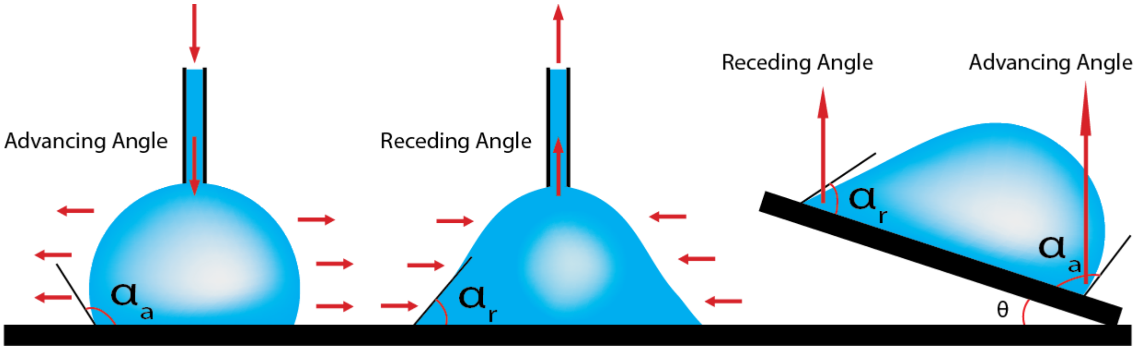

Figure 3 Illustration of the contact angle during the expanding and contracting the liquid or by the motion of the liquid droplet.

Water droplet of specific size can be used to evaluate surface adhesion by the sliding angle, which is the angle needed for a droplet to start sliding down from the tilted surface. Poor adhesion between the surface and the water droplets resulting to low sliding angle and vice versa. The difference between the advancing angle and the receding angle is called the hysteresis (H), which is given by equation (2.1).

$$H = \alpha_a - \alpha_r \tag{2.1}$$

Surface roughness and/or heterogeneity are the reasons of causing contact angle hysteresis. If the surface topography mainly affect the generation of the contact angle hysteresis, in this case, contact angles from the Young's equation can be misleading since it doesn't take surface roughness into the consideration [18]. Hysteresis is also one of the important parameters that asses the hydrophobicity of the surface. In general, low hysteresis can contribute to the hydrophobicity and self-cleaning effect, but surfaces with high advancing angle but low receding angle may show poor hydrophobicity and leave water drops “pinned” onto the surface [19]. Equation (2.2) [20] describes the force required for a droplet start to sliding on the solid surface. In the equation (2.2), where F is the critical line force per unit length of the drop perimeter, θ is the sliding angle. From the equation (2.2) one can see that hydrophobicity determined by the hysteresis rather than their finite values and it also indicates that a surface with very low hysteresis also will have a very low sliding angle, regardless of the magnitudes of the different contact angles [19].

$$\mathrm{F} = \gamma_{LV}(cos\theta_R - cos\theta_A) \tag{2.2}$$

Usually, on the rough solid surface, there is no reasonable relationship between the Young’s contact angle $\alpha_Y$, advancing contact angle $\alpha_a$ and receding contact angle $\alpha_r$ [21]. Basically, on the rough and heterogeneous surfaces, water droplet can exist in two kinds of equilibrium states, which are called Cassie-Baxter state [22] and Wenzel state [23], which are illustrated in Figure 4.

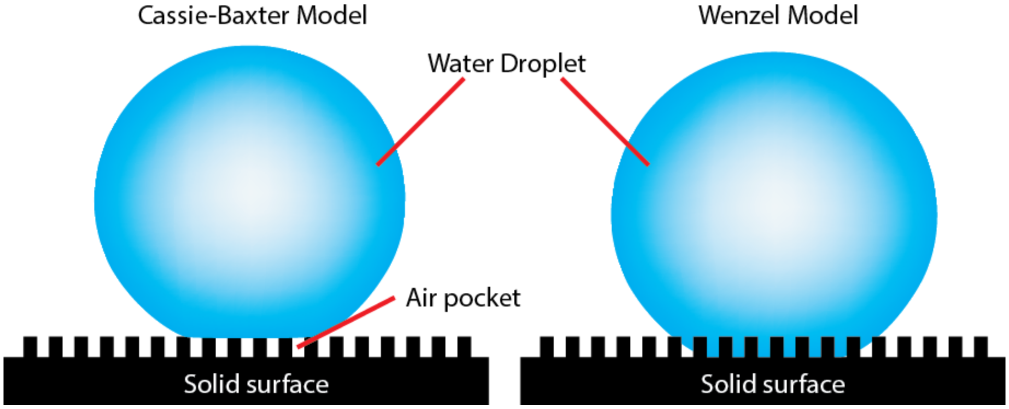

Figure 4 Cassie-Baxter model and Wenzel model

According to the simulation done by Johnson and Dettre [24] using an assumed sinusoidal surface structure, as increasing surface roughness the dominant hydrophobicity mode is continuously transformed from Wenzel state to Cassie-Baxter state. If hydrophobicity is only governed by the Wenzel state, even static contact angle is high enough, droplet may settle on the surface even when the surface is tilted until vertical. If hydrophobicity is only governed by the Cassie-Baxter state, even static contact angle is not very high,  droplet may starts sliding when the surface is tilted much less than the previous case angle [25]. Dynamic wettability strongly related to contact angle hysteresis and not the static contact angle. For a water-repellant surface, its dynamic wettability is very important factor [26].

## 2.2 Insight into the hydrophobic surfaces

Water contact angle on the surface is determined by both the chemistry of the surface and its roughness. A number of techniques were used to fabricate superhydrophobic surface by combining alteration of the surface chemistry with tuning the surface roughness. Rao et al. [12] reported that the change in the contact angle was dominated by the surface chemistry modification rather than the surface roughness alteration. Development of controlled hierarchical rough surface has been achieved by mimicking the surface roughness of the insect’s wing or self-cleaning lotus leaves. The surface structure of the developed rough surface enables entrapment of air between water droplets and the surface as in the Cassie-Baxter state. As shown in the Figure 4，in the case of Cassie-Baxter state, actual contact area between the solid surface and water droplet is much less than the Wenzel state. This contributes to less wetting and adherence between the surface and water droplets, thus creating a highly water repellent surface when combined with low surface energy.

## 2.3 Effect of surface roughness

It is a known fact that the hydrophobicity increased with surface roughness [22], [23]. Researchers have developed fractal surface with enhanced hydrophobicity [27] incorporating different surface structures [28][29][30]. It is however difficult to correlate and draw precise conclusions concerning the factors of surface roughness and the relationships between these factors.

Didem Oner et al. [22] prepared surfaces containing square spots of different sizes. They found that spots with X-Y dimensions of 32 μm and blow exhibite superhydrophobic behavior with high advancing and receding contact angles. Yoshimitsu et al. [25] developed a series of pillar and groove structures and concluded that groove surface structure on the silicon wafer having lower water contact angle than pillar surface structure. This is mainly because of better water shedding nature of groove surface structure than the pillar surface structure. Budunoglu et al. [31]created micro and nanoscale roughness and resulted surface having contact angles up to 179° and sliding angles less than 5° associated with the thermal stability up to 500°C. Gao et al. [32] developed superhydrophobic surfaces with hierarchical structure using PDMS and silica particles deposited onto glass slide. The silica-PDMS film was deposited by using simple immersion method for 10 minutes. Two sizes of silica particles were used; 7 nm and 14 nm. They found that 14 nm particles sizes have higher contact angle than 7 nm particles size due to the regularity of its micro- and nano-structure. Silica particle-PDMS surface with 7 nm has more grooves and irregularities which minimize the amount of air pockets to maintain the water droplet. Even, the hysteresis contact angle has shown similar trend with 10° for 14 nm particle and 40° for 7 nm particle size; the combination of 14 nm and 7 nm resulted in a hysteresis angle of 30°. Jin et al. [33] developed hierarchical-structured superhydrophobic surfaces using PDMS by casting and laser etching. The resulted surface texture is micro-submicron-nanostructures which is generated by micropillars and submicron-nano grooves and with static and dynamic water contact angles 162° and <5°, respectively.

## 2.4 Effect of surface chemistry

### 2.4.1 Surface energy

As mentioned above, Rao et al. [6] claimed that the higher contact angles are dominated by the surface chemical modification rather than the roughness of the surface. The contact angle of a liquid droplet on a smooth solid surface was described first by Thomas Young [34] who defined it by the mechanical equilibrium of the droplet under the action of three interfacial tensions shown in equation (2.3).

$$\gamma_{\mathrm{lv}}\mathrm{cos}\alpha_Y = \gamma_{\mathrm{sv}} - \gamma_{\mathrm{sl}} \; or \; cos\alpha_Y = \frac{\gamma_{sv} - \gamma_{sl}}{\gamma_{lv}} \qquad (2.3)$$

Where, $\gamma_{\mathrm{lv}}$ represents the liquid-vapor tension, $\gamma_{\mathrm{sv}}$ represents the solid-vapor tension and $\gamma_{\mathrm{sl}}$ represents the solid-liquid interfacial tensions, and $\alpha$ is the static contact angle. Table 1 provides the critical surface tension ($\gamma_{\mathrm{c}}$) values of surface functional groups in relation to surface constitution at 20°. From the table, it is clear that the surface functionalized by fluorocarbon group of $CF_3$ having lowest surface energy. Substitution of fluorine atoms by hydrogen atoms in $CF_3$ groups can increase the surface energy. Normally, to get low surface energy surface, functionalization of the surface by fluorocarbon groups is preferred as compared to hydrocarbon groups and chlorocarbon groups.

Table 1 Critical surface tension ($\gamma_c$) values in relation to surface constitution at 20° [35].

| **Surface groups** | **$\gamma_c$ (mN/m)** |
|---|---|
| **Fluorocarbon surfaces** | |
| $-CF_3$ | 6 |
| $-CF_2H$ | 15 |
| $-CF_2-CF_2-$ | 18 |
| $-CF_2-CFH$ | 22 |
| $-CF_2-CH_2-$ | 25 |
| $-CFH-CH_2-$ | 28 |
| **Hydrocarbon surfaces** | |
| $-CH_3$ (crystal) | 20-22 |
| $-CH_3$ (monolayer) | 22-24 |
| $-CH_2-CH_2-$ | 31 |
| $-CH-$ (phenyl ring edge) | 35 |
| **Chlorocarbon surfaces** | |
| $-CClH-CH_2-$ | 39 |
| $-CCl_2-CH_2-$ | 40 |
| $=CCl_2$ | 43 |

### 2.4.2 Silica/Silane chemistry

Silica ($SiO_2$) consists of tetrahedral $[SiO4]^{4-}$, which can be used to create surface roughness. Modification of the silica by low surface energy reagents leads to a low surface energy layer. Silanol (Si-OH) groups which can be hydrolyzed through hydrolysis reaction and low surface energy functional groups connected through condensation reaction. Silica is usually utilized in the form of colloid dispersion, or silica nanoparticles among which solid silica particles suspended in an aqueous phase and silica nanoparticles dispersed in proper solvent, named by silica sols. Silica sols can be used in Solution-Gelation (Sol-Gel) reactions, where reaction usually go through the hydrolysis and condensation process used to create oxide network structures with the surface functionalized by low surface energy functional groups.

It is known that unmodified silica aerogel surface having hydrolysable silanol (Si-OH) groups. Hydroxyl (-OH) groups hydrophilic characteristic is the main source of hydrophilicity, because presence of this group adsorption of the water will be promoted. Silica aerogel surface also shows hydrophilicity[36] and not favorable for the hydrophobicity. Therefore, silanol (Si-OH) replaced by the more hydrolytically stable silicon alkyl (Si-R or Si-$CH_3$) groups resulted in surface of aerogel with low energy and the adsorption of the water also inhibited. This is very important when dealing with liquid/solid interfacial energy [35]. Figure 5 is a schematic diagram showing replacement of hydrophilic groups by hydrophobic groups. Furthermore, macroporous structures of aerogel are potential scaffolds for immobilization of biological species [37]. They also can create like Lotus Leaf Effect with the entrapment of the air in the surface roughness asperities valleys.

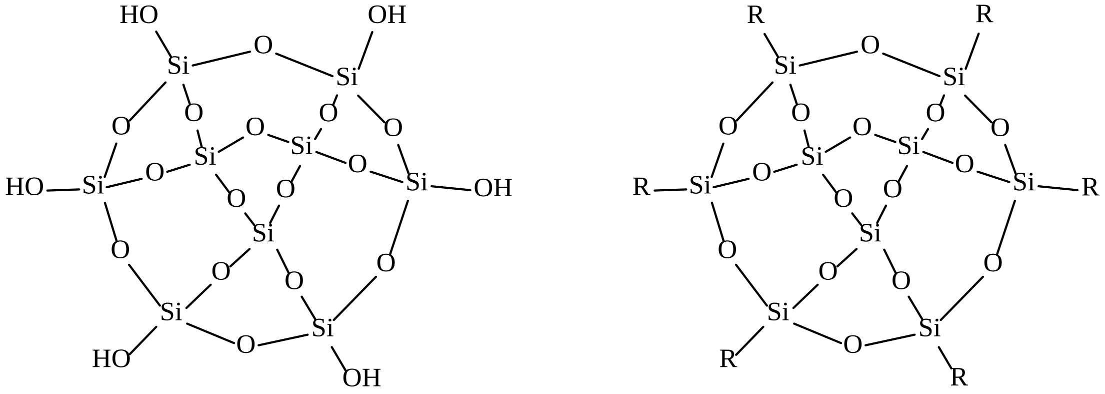

Hydrophilic Hydrophobic

Figure 5 Schematic diagram showing hydrophilic and hydrophobic surfaces of silica aerogels [38]

The schematics shown below illustrate the basic concept of sol-gel reaction.

Hydrolysis reaction of silane:

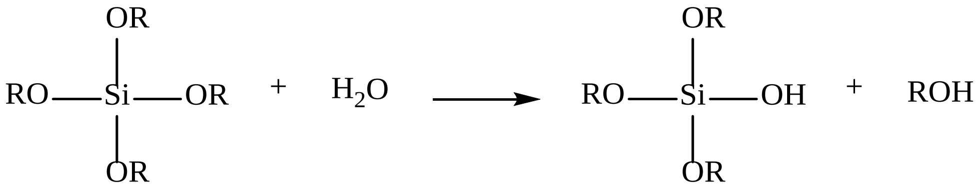

$$\mathrm{Si(OR)_3OR} + H_2O \longrightarrow \mathrm{Si(OR)_3OH} + \mathrm{ROH}$$

Water Condensation:

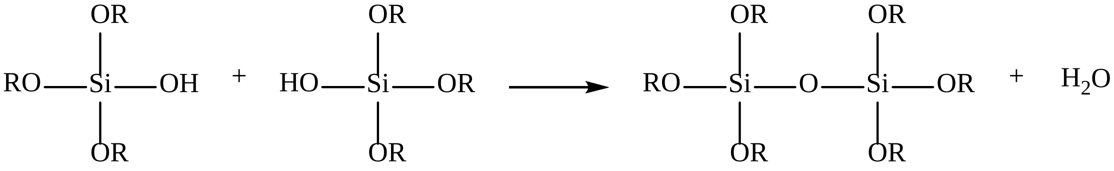

$$\mathrm{(RO)_3Si{-}OH} + \mathrm{HO{-}Si(OR)_3} \longrightarrow \mathrm{(RO)_3Si{-}O{-}Si(OR)_3} + H_2O$$

Alcohol condensation:

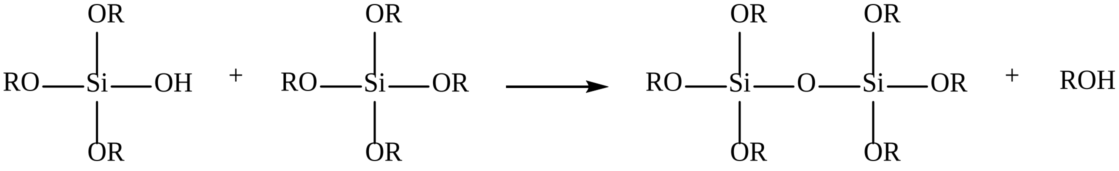

$$\mathrm{(RO)_3Si{-}OH} + \mathrm{RO{-}Si(OR)_3} \longrightarrow \mathrm{(RO)_3Si{-}O{-}Si(OR)_3} + \mathrm{ROH}$$

If we take the hydrolysis and condensation reactions of methyltrimethoxysilane (MTMS) as an example.

Hydrolysis:

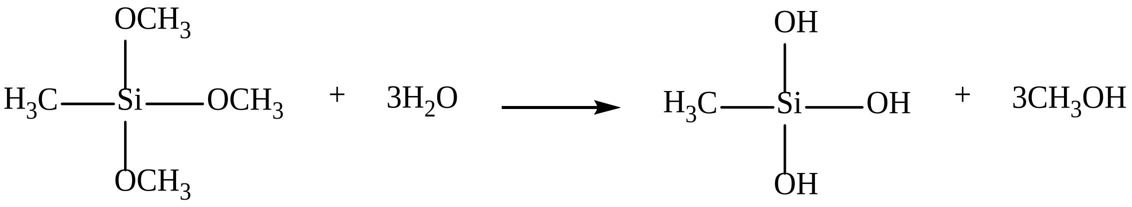

$$H_3C{-}Si(OCH_3)_2{-}OCH_3 + 3H_2O \longrightarrow H_3C{-}Si(OH)_2{-}OH + 3CH_3OH$$

Water condensation:

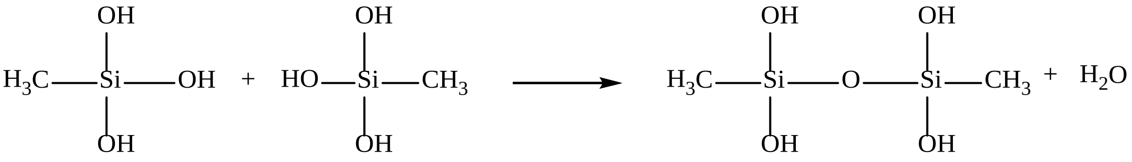

$$H_3C{-}Si(OH)_2{-}OH + HO{-}Si(OH)_2{-}CH_3 \longrightarrow H_3C{-}Si(OH)_2{-}O{-}Si(OH)_2{-}CH_3 + H_2O$$

Alcohol condensation:

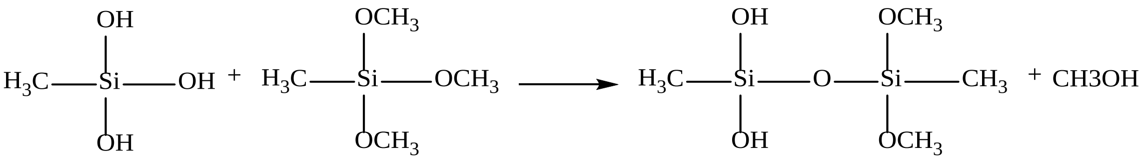

$$H_3C{-}Si(OH)_2{-}OH + H_3C{-}Si(OCH_3)_2{-}OCH_3 \longrightarrow H_3C{-}Si(OH)_2{-}O{-}Si(OCH_3)_2{-}CH_3 + CH3OH$$

For this case, as each monomer contains three hydrolyzable Si–OH or Si–$OCH_3$ groups, it can form 3D gel network after a series of reactions. The surface of the cluster would mostly be covered by these low surface energy Si–$CH_3$ groups. After the completion of condensation reactions, then the surface of the aerogel becomes hydrophobic, which is ascribed to one non-hydrolysable Si–$CH_3$ group in each monomer of MTMS [10]. Therefore, by this sol-gel chemistry reactions silica particles can be easily functionalized with low surface energy and hydrophobic functional groups by different kinds of silanes.

Figure 6 shows the Organically Modified Silanes with different functionalities. A number of these functionalities in the monomer can have different significance during the sol-gel reactions. A tetra-functional silicon alkoxide (n = 0) acts as a “network forming” structure since it has for hydrolyzable sites. A trifunctional silicon alkoxide (n = 1) behaves as a “cross-linker” with its three hydrolyzable sites. A difunctional silicon alkoxide (n = 2) having two hydrolyzable sites and behaves as a “ bridging ” agent and a monofunctional silicon alkoxide (n = 4) can be used as a “ terminating ” agent, since it has only one site can take part in the reactions [39].

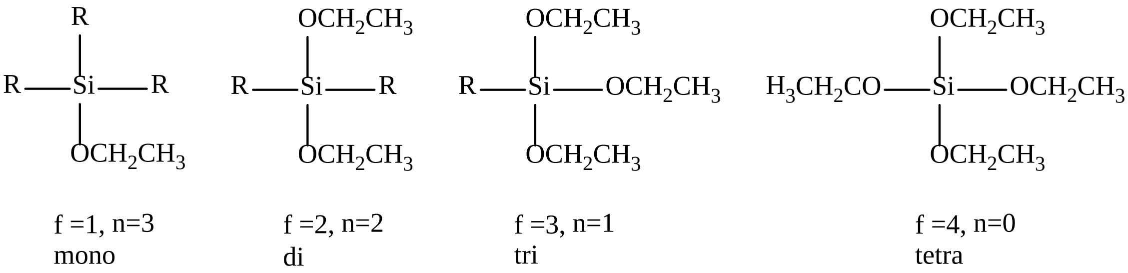

Figure 6 Organically modified silica (ORMOSIL) functionalities.

## 2.5 Fabrication of superhydrophobic surfaces – drawbacks

Some researchers reported that by using commercially available abrasion resistance silicone resin improves the abrasion resistance of the superhydrophobic surfaces [40], [41]. This is often used with a coupling/bonding agent to increase the adhesion between the substrate and thin layers [16]. Water-repellent surfaces prepared by sol-gel route suffer from some major drawbacks that severely limit their large scale outdoor applications. The most notable of these are poor mechanical properties that include weak adhesion to substrate and low wear/abrasion resistance, and fast degradation under UV radiation due to vulnerability to long-term UV exposure of polymers. In this regard, development of water-repellent surfaces with improved mechanical stability/robustness and good resistance to long-term UV weathering are the major challenges. Hence in depth research is needed to address these issues and overcome the above mentioned challenges as well as not compromising on the transparency.

## 2.6 Research objectives

The main objectives of the present research are:

1. Development of optically transparent, water-repellent and self-cleaning surfaces using surface modified silica nanoparticles through sol-gel method. Silica nanoparticles to be used to increase the surface roughness and PFOTS used to functionalize the surface of silica nanoparticles.
2. Improvement of the mechanical properties (adhesion to substrate, abrasion/wear resistance, scratch resistance etc.) of the developed surfaces by controlled addition of bonding agents. Since the aim of developed surfaces are for outdoor field applications, developed surfaces will be tested under simulated conditions, such as UV light, water jet, sand paper abrasion and sand blasting test.
3. Optimization of the process parameters and conditions to obtain the best combination of the above desired characteristics.

# CHAPTER 3

# MATERIALS AND METHODOLOGY

## 3.1 Materials

The materials used to fabricate the intended robust superhydophobic and self-cleaning surfaces are: 1) Silicon dioxide (nanopowder, 10-20 nm particle size (BET), 99.5% trace metals basis), 2) Methyltrimethoxysilane (MTMS), (3-Glycidyloxypropyl) trimethoxysilane (GLYMO), 1H,1H,2H,2H-Perfluorooctyl-trichlorosilane (PFOTS), 3) ethanol, 4) acetone, 5) Ammonia (30 Vol%). All of these chemicals were purchased from Sigma-Aldrich, Germany. Figure 6 shows the molecular structure of the MTMS, GLYMO and PFOTS used in our experiments. The deionized (DI) water used during the experiment was collected from the Milli-DI® Water Purification System.

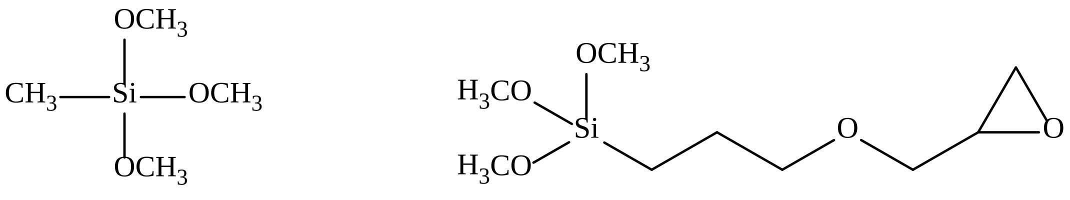

(a) MTMS (b) GLYMO

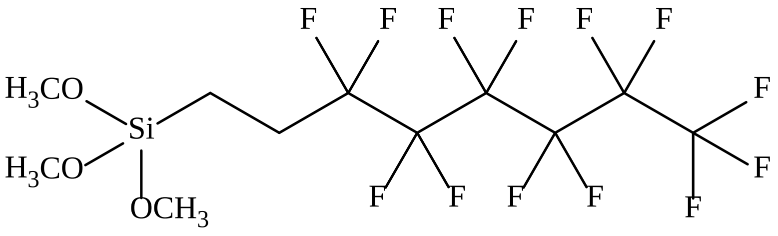

(c) PFOTS

Figure 7 Molecular structure of (a) MTMS, (b) GLYMO, (c) PFOTS

## 3.2 Fabrication of superhydrophobic surfaces

### 3.2.1 Preparation of the coating solution

The coatings are prepared by the sol-gel method which has recently become a popular choice among researchers due to its advantages over contemporary techniques [39], [42]. Basically, the sol-gel process is the transition of a system from a liquid solution ("sol") into a semi-solid gelation ("gel") phase.

Coating solution A (referred to as Sol A) is prepared by adding the following chemicals into the beaker during magnetic stirring at a constant speed throughout the synthesis process. Molar ratio of GLYMO: MTMS: DI=1:2:9 adopted which is corresponding to the amount of Ethanol (10 ml), Ammonia (0.5ml), GLYMO (2 ml), MTMS (2.58 ml) and DI water (1.47 ml). All of these chemicals were added to the beaker dropwise meanwhile stirring with magnetic stirrer. Beaker covered with the Aluminum foil to avoid reduction of solution by evaporation and solution stirred for 1 hour. After preparation of sol A, it was used immediately after 1 hour of stirring, otherwise after few hours or few days, the sol A becomes gel depending upon the amount of $NH_4OH$ catalysis was added to Sol A. Below Figure 8 showing how Sol A bonding with glass surface. First of all, both MTMS and GLYMO in Sol A have three hydrolysable methoxy groups (-OCH3) sites hydrolyzed and substituted by hydroxyl groups (-OH). Hydroxyl groups on MTMS, GLYMO and glass through condensation reaction chemically bonded.

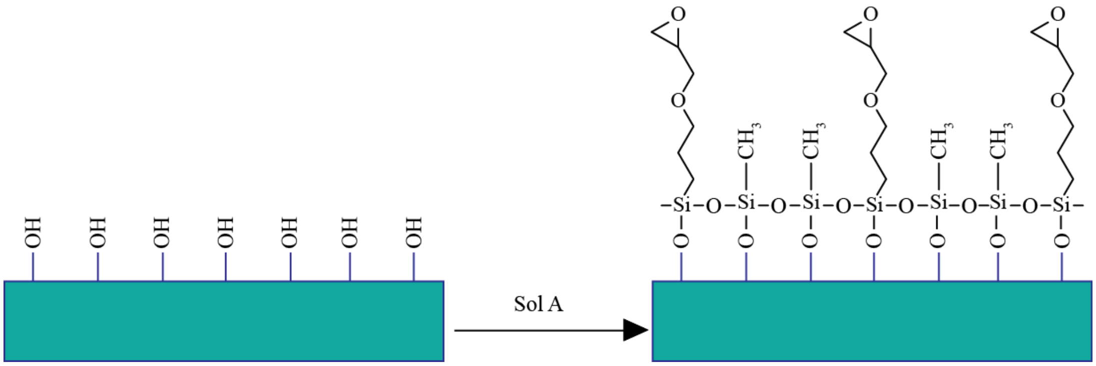

Figure 8 Schematic of MTMS and GLYMO in solution A bonding with Glass surface.

Coating sol B prepared with different weight percentage of silica nanoparticles functionalized by PFOTS in the ethanol as a solvent. Below Figure 9 showing the schematic of functionalized silica particles by PFOTS.

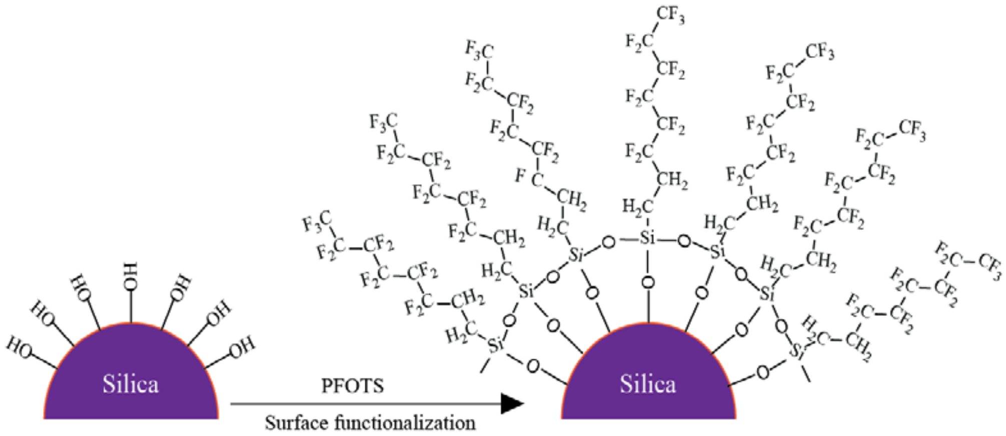

Figure 9 Schematic of functionalization of silica particles by PFOTS.

Sol B with different percentage of silica was prepared as presented in the Table 2**.** Sol B consisting of ethanol, PFOTS and different weight percentage of silica sonicated in the ultrasonic bath for 2 hours. Sol B was kept in sealed bottle and was used as second layer after first layer of Sol A.

Table 2 Solution B composition for different weight percentage of silica.

| SiO2 wt% in Sol B | Ethanol (g) | Silica (g) | PFOTS (g) |
|---|---|---|---|
| **0 wt%** | 9.8 | 0 | 0.2 |
| **0.5 wt%** | 9.75 | 0.05 | 0.2 |
| **1.0 wt%** | 9.7 | 0.1 | 0.2 |
| **2.0 wt%** | 9.6 | 0.2 | 0.2 |

### 3.2.2 Deposition of the hydrophobic films

Prior to spray coating, new glass slides were cut into 25×25 mm pieces and thoroughly cleaned by first sonicating them in acetone followed by DI water for 10 minutes each then dried before spray coating them.

The spray coating process was performed by BADGER NO 150 (USA) spray gun and the setup is illustrated in Figure 10 (a). First, the jar containing Sol A was connected to the spray gun with the gas inlet connected to nitrogen cylinder to apply constant pressure of 300 kPa during the spray coating process. The distance between the glass slides and spray gun tip was also one of the important parameter that can affect the uniformity of the film deposited on the glass substrate surface. If the spray gun is too far, sprayed solution will be wasted before reaching the surface of the glass under constant pressure. If the spray gun is too near, sprayed solution concentrates on the center of the surface. Thus, proper spray distance was chosen for getting uniform film on glass surface. First, distance optimized to 15 cm then Sol A was sprayed on the glass slides with 3 cycles.

After glass slides was coated with Sol A, samples were carefully put in the oven at 80 °C for 2 hours to evaporate the ethanol solvent completely.

One spray cycle defined as follows: first step, glass substrate was fixed vertically as showed in Figure 10 (a). Spray gun was manually traveled from right/left side to left/right side of glass, solution was deposited on the glass surface during the spray gun travel (scan) through on it.

After complete curing of the first layer Sol A, the glass slides were immediately sprayed with second layer of Sol B to functionalize the surface as well as to increase the roughness; schematic illustration of the process shown in Figure 10 (b). After completion of the surface modification, the glass substrate can either be cured at a certain temperature for certain time or kept at room temperature for 24 hours. In both cases, the PFOTS molecules need time to re-arrange their molecules to reach thermodynamic stable state [43]. In this study, glass slides were kept at room temperature for 24 hours after the deposition of second layer of Sol B. After this process, the surface becomes chemically stable and water contact angle measurements can be conducted. It is worth mentioning that the second layer which is Sol B should be immediately deposited after curing of the first layer. This is to avoid oxidation of the functional groups such as –OH of the first layer which are responsible for the condensation reaction that occurs between the two different layers.

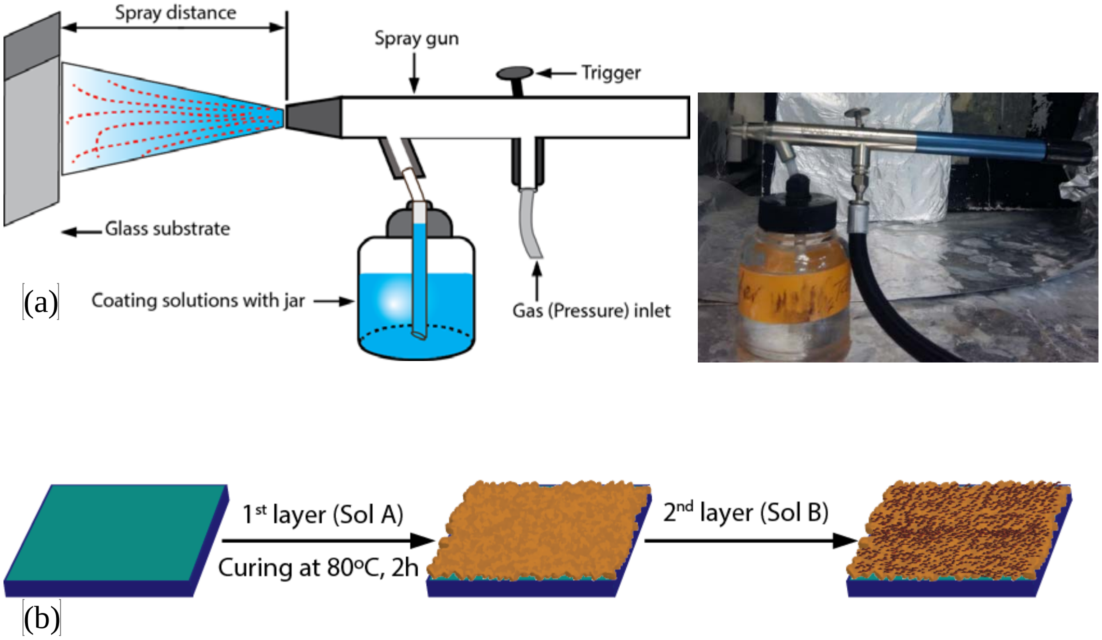

Figure 10 (a) Spray coating setup illustration and actual spray gun used in the experiment, (b) schematic illustration of solution A and solution B applied on glass surface.

After the deposition of the second layer Sol B which consists of silica nanoparticles surface functionalized by PFOTS, the samples were cured at certain temperature for specific time period. Thereafter, they were maintained at the room temperature for longer time to enable the proper alignment and arrangement of low surface energy -$CF_2$, -$CF_3$ functional groups to the surface as reported in the literature [43]. Usually, it takes approximately up to 24 hours for PFOTS to rearrange itself so that low surface energy groups such as -$CF_3$ get arranged outward decreasing the total surface energy of the coating layer. As illustrated in the Figure 11, first layer coating bonded with glass surface. Second layer of functionalized silica nanoparticles imbedded in the first layer coating.

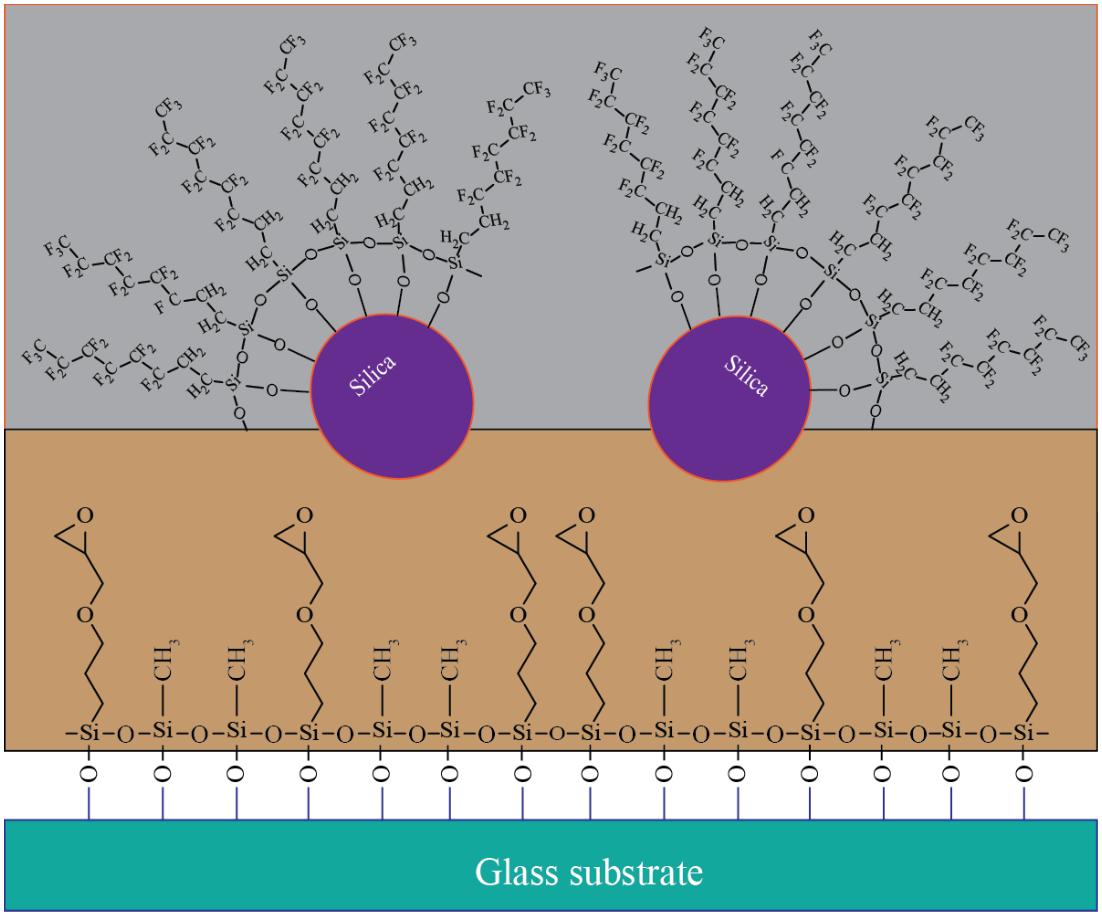

Figure 11 Schematic of two layers of coating solution on glass surface

In our study, annealing at 60°C for 3 hours, annealing at 80°C for 2 hours, or even keeping it at room temperature for approximately 24 hours, showed similar results. If the water contact angle was measured directly after application of second layer Sol B without annealing or waiting at room temperature for approximately 24 hours, the angle decreased with time and a transition from superhydrophobic to hydrophilic behavior was observed within very short time. It took only a few minutes for the contact angle to decrease from more than 150° to approximately 90° or below.

Table 3 gives the nomenclature for the samples coated with second layer of Sol B with different weight percentage of silica and different spraying cycles (1-5 cycles).

Table 3 Samples identification (name) according to silica weight percentage and spray cycles.

| **SiO2 wt%** | **Spray cycles** | | | | |
|---|---|---|---|---|---|
| | **1** | **2** | **3** | **4** | **5** |
| **0** | B0-1 | B0-2 | B0-3 | B0-4 | B0-5 |
| **0.5** | B0.5-1 | B0.5-2 | B0.5-3 | B0.5-4 | B0.5-4 |
| **1.0** | B1-1 | B1-2 | B1-3 | B1-4 | B1-5 |
| **2.0** | B2-1 | B2-2 | B2-3 | — | — |

## 3.3 Characterizations

A contact angle goniometer (Kyowa Interface, Inc. Japan) was used to determine the static water contact angle, sliding angle, advancing and receding contact angle (Figure 2 and Figure 3 shown earlier). The hysteresis was calculated according to equation (2.1). The sessile drop model was used with the tangential method to measure the static water contact angles in a proper manner. Approximately 10 μl water droplets were carefully placed on the surface and the angle was measured from the captured image. Measurements, from different locations on the surface, were repeated at least 5 times for each sample to obtain an average value that was representative for the sample.

UV-VIS spectrophotometer (JASCO, V-670) was used to measure the transmittance of the spray coated glass slides in the visible light wavelength range of 400 to 780 nm as shown in Figure 12. Transmittance of the surface to visible light is crucial for the fabricated surface since the intended use is mainly for self-cleaning of Solar PV panels.

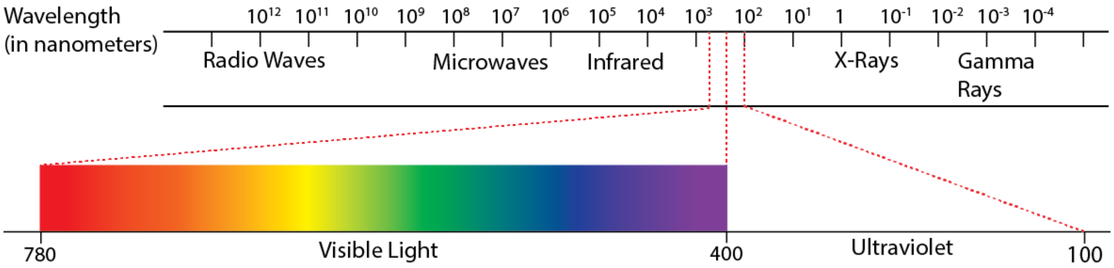

Figure 12 Wavelength of visible light and ultraviolet.

Surface morphology was studied with a field emission scanning electron microscope (FESEM, TESCAN). Prior to analysis, the samples were coated with gold to make the surfaces electrically conductive. The elemental composition of selected locations was analyzed using Energy Dispersive Spectroscopy (EDS).

Surface topography was characterized by 3D optical microscopy (Bruker Inc. Germany). Each of the samples analyzed at 3 different locations and the average value is reported.

The Raman spectra of selected samples were recorded with DXR Raman Spectrometer (Thermo Scientific) using a 455 nm laser source. By analyzing the Raman spectra functional groups presented at the surface examined and confirmed.

FTIR spectra were obtained using a Nicolet is50 spectrometer (Thermo Scientific) with an ATR accessory. FTIR spectra was used to analyze the functional groups presented on the surface. FTIR spectra was also used to determine the functional groups at different annealing temperature and effect of annealing can be examined.

X-ray Photoelectron Spectroscopy (XPS) was carried out to determine the surface atomic concentration. The data were collected on a Thermo Escalab 250 probe system equipped with an aluminum anode to produce a focused X-ray beam. The diameter of the X-ray spot was about 500 µm. The equipment contained a spherical capacitor energy analyzer and a multichannel detector. Surface survey scans were collected, followed by high resolution scans for Carbon, Oxygen, Silicon and Fluorine.

## 3.4 Durability and Robustness Tests

### 3.4.1 Ultraviolet resistance test

OmniCure S2000 UV spot curing system (EXCELITAS TECHNOLOGIES) was used to study the UV resistance of the coating and OmniCure R2000 radiometer was employed to measure the light intensity reaching the surface of the coated glass substrate.

Samples going to be tested were placed under the UV light source and a radiometer was used to measure the light intensity that reached sample surface. Figure 13 (a) Power spectra of the OmniCure S2000 UV lamps, Figure 13(b) showing illustration of Sample placed under the UV light for testing the UV resistance. Sample B1-3 was tested under a UV light intensity of 2500 $W/m^2$ (250 $mW/cm^2$) for 10 hours and followed by exposure to a very high UV light intensity of 30000 $W/m^2$ (3000 $mW/cm^2$) for 2 hours.

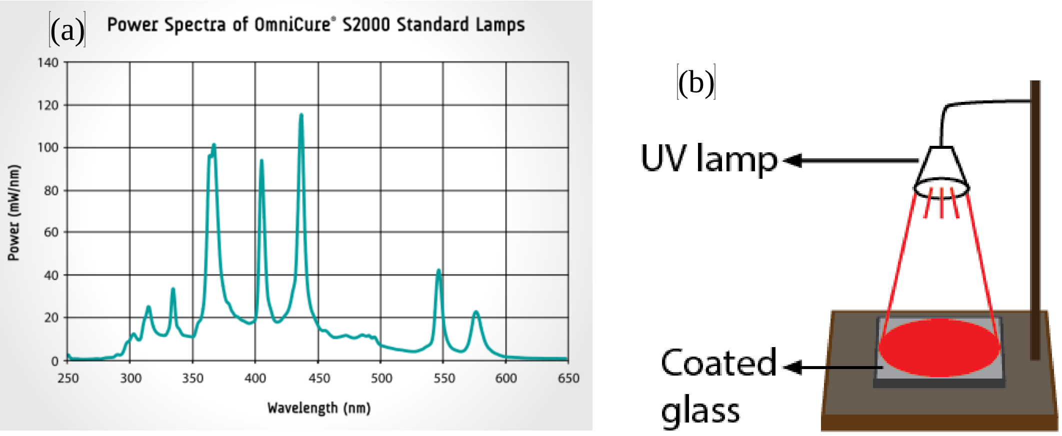

Figure 13 (a) Ultraviolet lamp power spectra (b) Illustration of coated samples tested under ultraviolet light.

### 3.4.2 Thermal stability test

Selected sample B1-3 tested for thermal stability at different temperature of 300°C, 350 °C and 400°C. First, oven was heated to the intended temperature then at least three samples of b1-3 for each temperature placed in the oven for 2 hours annealing. After annealing, all the samples contact angle were measured and characterized by FTIR.

### 3.4.3 Water jet test

Water jet test schematic is illustrated in Figure 14. Water was flow continuously at the rate of 1L/min through a 4mm diameter tube impacting the surface. Coated glass was placed under water jet for 1hour and total volume of 60L water was consumed during the water jet test. Adjustable stick was properly adjusted so that distance between water tube tip to surface of the glass was tested which is D2 adjusted to 15cm and D1 about 10 cm as showed in the illustration.

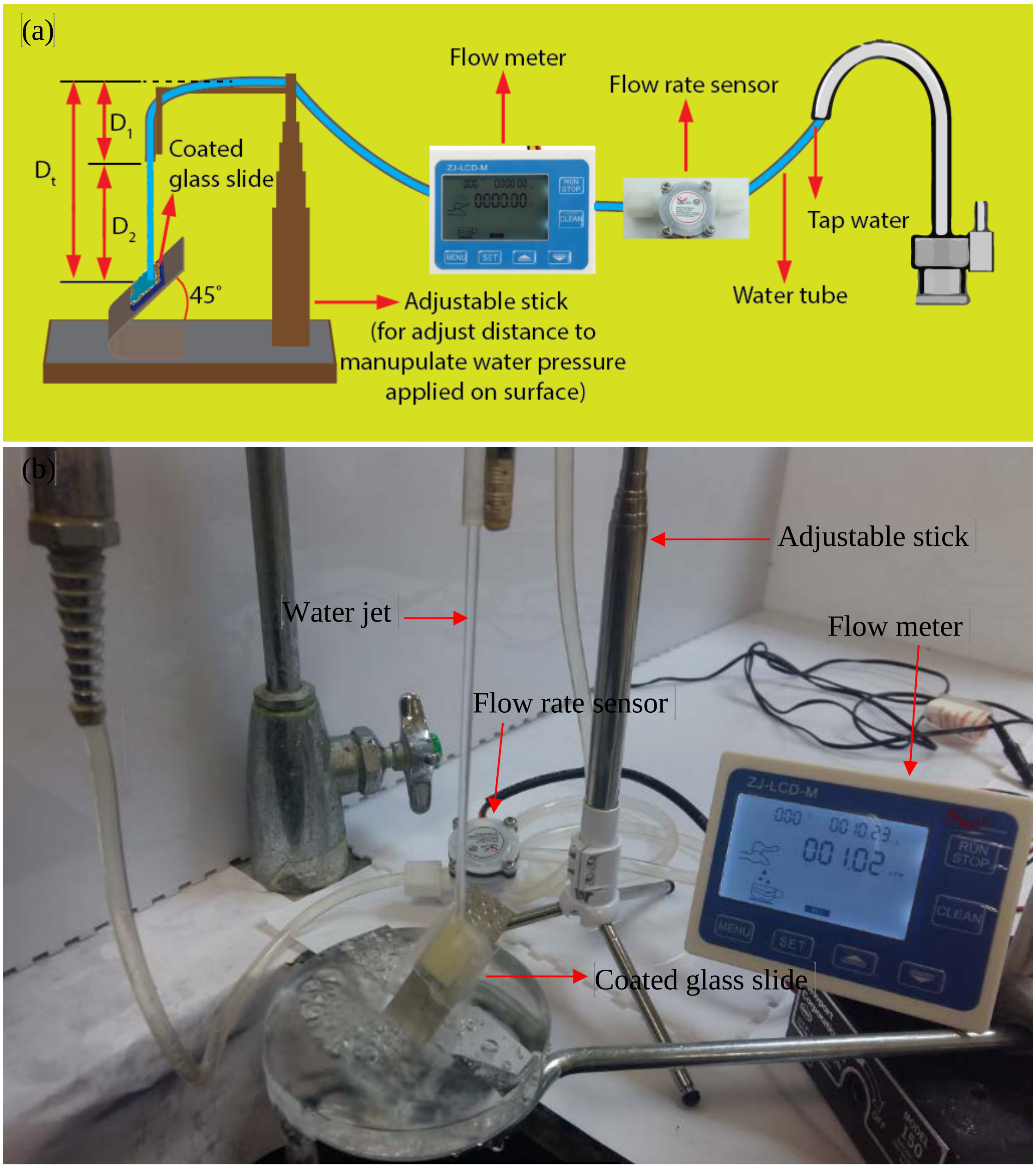

Figure 14 Specially designed water jet test setup (a) illustration of the assembly of the setup, (b) actual water jet test setup

### 3.4.4 Abrasion resistance test

Sample was placed on the BUEHLER 240 GRIT size sand paper with the coated surface in contact with the sand paper and on top of glass surface placed 100g of weight. Abrasion test was conducted as illustrated in Figure 15. In the first step, the sample traveled a distance of 10 cm on the sand paper and the glass slide horizontally was rotated 90°. In the second step, it traveled back to original position with traveling distance of 10 cm. These two steps were considered as one cycle. Total of 5 cycles of abrasion test were conducted that is corresponds to a total traveling distance of 100 cm. According to the glass piece size of 25×25 mm and 100 g of weight on it, applied pressure on the surface during the test was about 1.6 kPa.

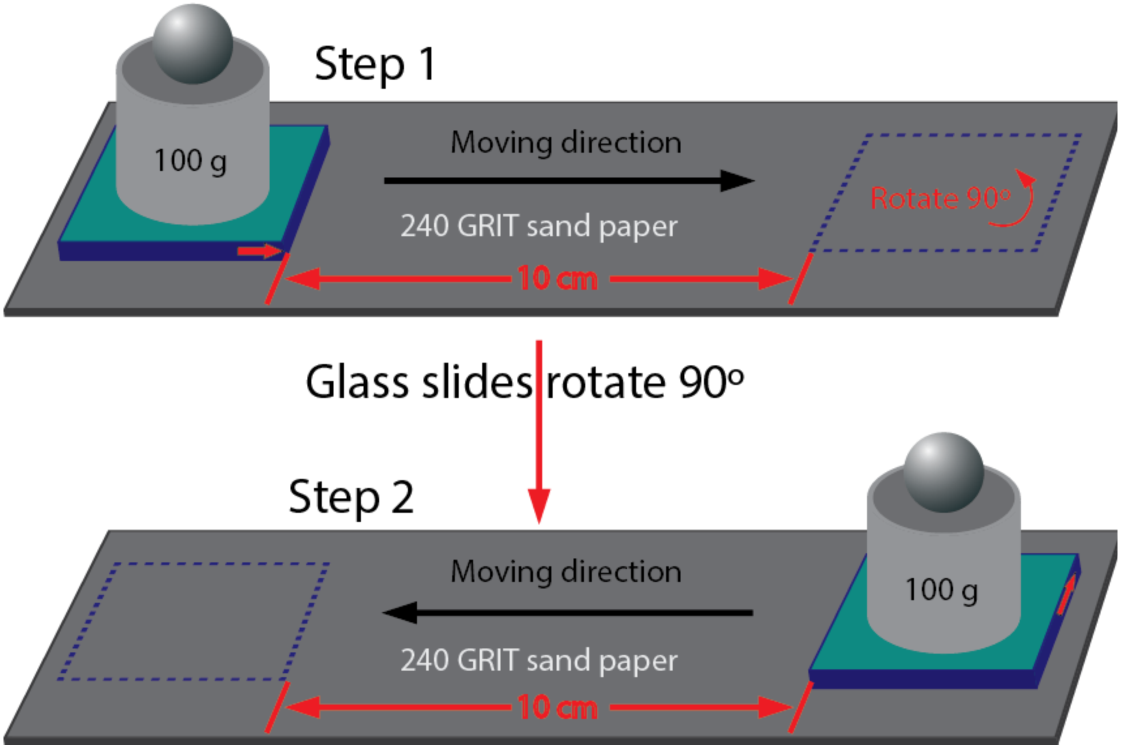

Figure 15 Abrasion test on the 240 GRIT sandpaper

### 3.4.5 Sand blasting test

An air pressure of approximately 300 kPa was applied to blow sand through a 6 mm nozzle opening. Sample surface to nozzle tip distance was adjusted to about 15 cm. As shown in Figure 16, sand particles are continuously fed from the sand container and hitting the coated glass surface. More than 300 g of sand particles were blown on the surface in about 10 minutes duration.

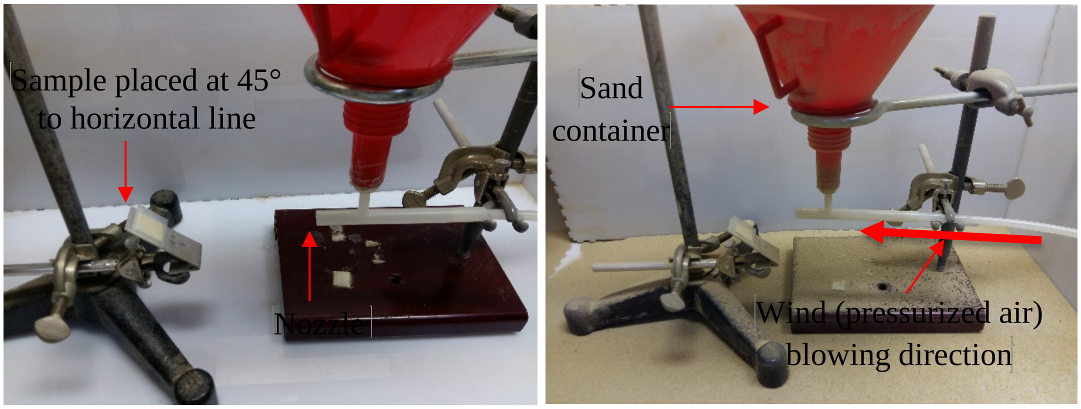

Figure 16 Specially designed sand blasting test setup.

# CHAPTER 4

# RESULTS AND DISCUSSION

## 4.1 Optimization of the spray coating parameters

For a uniform deposition of the coating solution on the glass surface, it is important to control the spray coating parameters within specific limits. Since transmittance of the glass substrate after the application of coating is crucial, each of the coating layer should be applied such that the decrease in transmittance is minimum. As mentioned in chapter two, spray gun distances (10 and 15 cm) and five cycles (layers) were considered. Figure 17 shows how each of the cycles (coating layers) of solution A affects the glass transmittance for both distances. Spraying of Sol A was performed immediately after 1 hour of stirring, otherwise Sol A viscosity increased and it transformed to gel with time as sol-gel reaction is taking place. As indicated in the Figure 17 (a) and (b), transmittance of coated glass with sol A (Sol A was sprayed after 24 hours after sol A prepared). It is obvious that the coating reduces the transmittance and the thicker the coating the lower the transmittance is. The application of first layer on the glass surface compromised the transmittance by more than 25% for 10-cm and more than 20% for 15 cm. The decrease in transmittance is ascribed to the high viscosity of the Sol A.

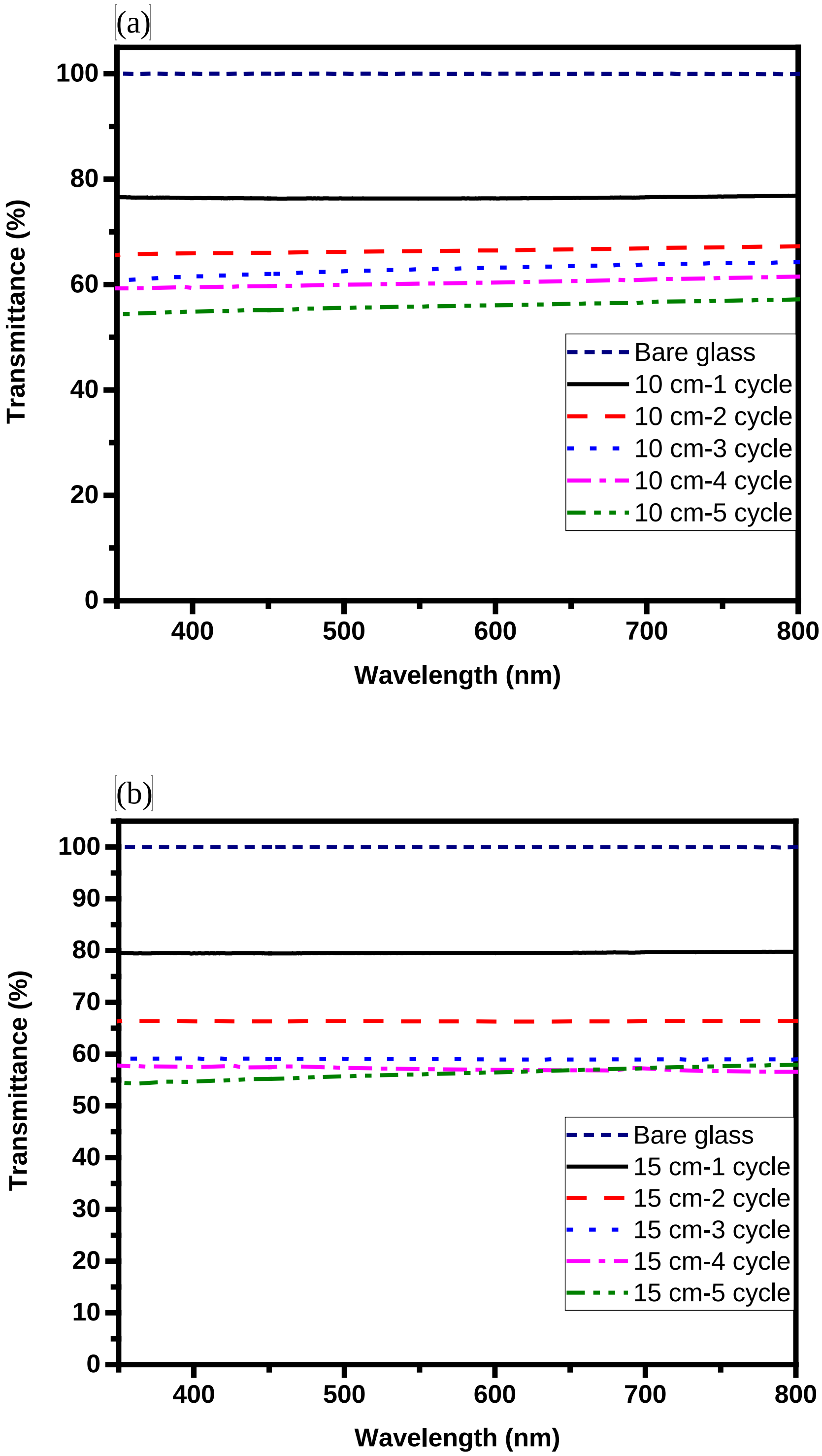

Figure 17 Transmittance of the glass coated with solution A (after 24 hours) (a) at spray distance of 10 cm (b) spray distance of 15 cm.

In general, spraying from a distance of 15 cm yielded better transmittance for all cycles when compared with the spraying distance of 10 cm. When highly viscous Sol A is sprayed over the glass surface, tiny droplets are formed rather than a continuous coating. This accounts for the decrease in the transmittance by approximately 20% at a 15 cm spray distance and only with one spray cycle. The results show that, to get a smooth first layer, Sol A should be sprayed immediately after synthesis process to avoid gelation which gives rise to high viscosity. Thus, Sol A was sprayed immediately after the synthesis process from a distance of 15 cm. Figure 18 shows how this optical property is improved by the optimized parameters.  The decrease in transmittance of the glass could be maintained at levels which are within 2-3% of that of the bare glass. By comparing Figure 17 and Figure 18 it can be concluded that the viscosity of the solution affects the spray coating process and spraying of the viscous solution may form tiny droplets on the surface rather than uniformly spread over the glass surface and increased the light reflectance. To avoid compromising on transmittance of the glass, sol A was used right after it prepared before sol A. It is evident from our experiment that, significant increase in viscosity should be avoided.

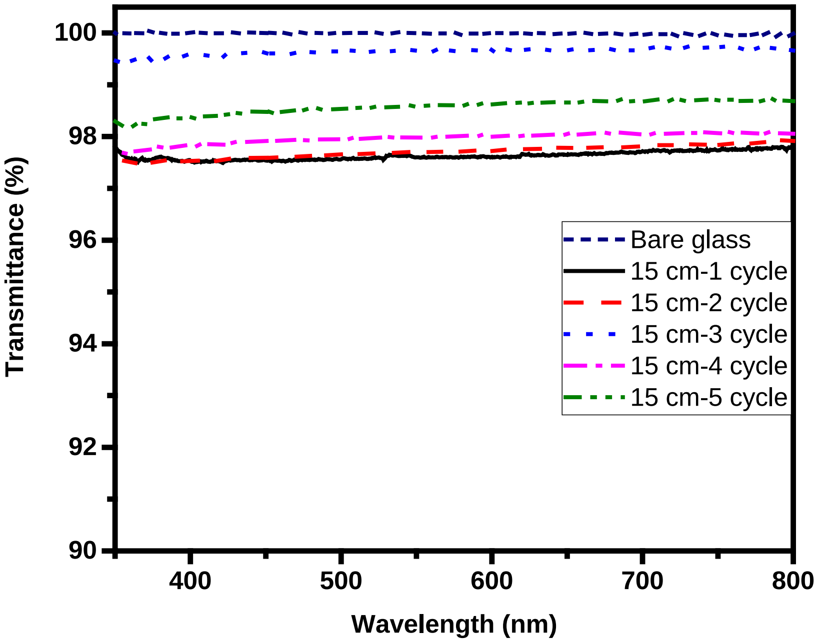

Figure 18 transmittance of the glass spray coated with solution A (immediately) at 15 cm spray distance.

Based on Figure 17 and Figure 18, it was decided to 3 cycles of Sol A with pressure of 300 kPa and at a spray distance of 15 cm. It is clear from the Figure 18, that transmittance of 3 cycles is very close to glass. Similar to application of sol A, for application of sol B, spray pressure of 300 kPa and spray distance of 15 cm was adopted.

## 4.2 Effect of silica nanoparticles on hydrophobicity and transmittance

Following the optimization of spraying process of Sol A in terms of optical properties, the coating hydrophobicity is studied.

The second layer of Sol B with different weight percentage (0%, 0.5%, 1.0% and 2.0%) of silica Nanoparticles was sprayed on the surface immediately after curing of first layer. Static, sliding, advancing, receding angles and hysteresis were measured properly. When the water droplet on the surface start sliding within the tilting degree of 30° then the sliding angle, advancing angle, receding angle and hysteresis were reported otherwise only static water contact angle was reported and other details reported as a NA (Not Available).

Table 4 Contact angle of the samples sprayed with Solution B without silica Nanoparticles.

| **Samples** | **CA** | **SA** | **Advancing Angle (AA)** | **Receding Angle (RA)** | **Hysteresis(H)** |
|---|---|---|---|---|---|
| **B0-1** | 108.5±1.8 | NA | NA | NA | NA |
| **B0-2** | 110.2±1.1 | NA | NA | NA | NA |
| **B0-3** | 111.6±0.7 | NA | NA | NA | NA |
| **B0-4** | 113.8±1.4 | NA | NA | NA | NA |
| **B0-5** | 114.2±1.1 | NA | NA | NA | NA |

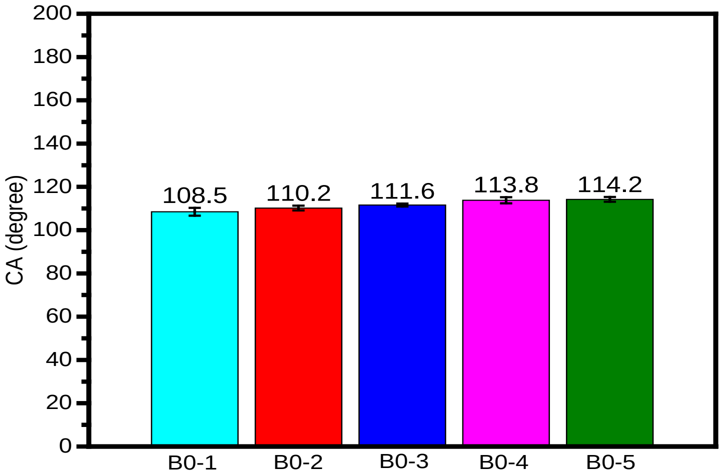

Figure 19 Contact angle of the samples sprayed with Solution B without silica Nanoparticles.

When the second layer applied without silica nanoparticles, there is no significant change in the static contact angle with the increase of the spray cycles. This results indicating that even 1 to 2 cycles spraying of second layer Sol B can be enough for the functionalization of the surface with low surface energy functional groups. Only by modifying the surface chemistry highest reported static water contact angle did not exceed 120° without inducing roughness. This results are also in accordance with results reported in some literatures [39].

Table 5 Contact angle of the samples sprayed with Solution B including 0.5 wt% silica Nanoparticles.

| **Samples** | **CA** | **SA** | **Advancing Angle (AA)** | **Receding Angle (RA)** | **Hysteresis(H)** |
|---|---|---|---|---|---|
| **B0.5-1** | 117.9±2.8 | NA | NA | NA | NA |
| **B0.5-2** | 121.3±3.6 | NA | NA | NA | NA |
| **B0.5-3** | 129.9±3.7 | NA | NA | NA | NA |
| **B0.5-4** | 138.6±2.3 | NA | NA | NA | NA |
| **B0.5-5** | 144.0±2.4 | 18.8±4.3 | 146.2±2.9 | 120.7±7.9 | 25.5±7.3 |

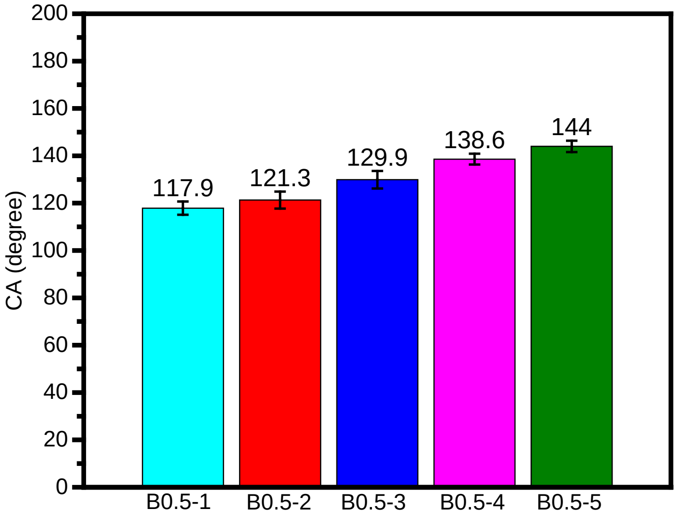

Figure 20 Contact angle of the samples sprayed with solution B including 0.5 wt% silica Nanoparticles.

Figure 20 shows that addition of the 0.5 wt% silica nanoparticles to Sol B, static CA increased by about 10° (from 108 to 118º) when Sol B sprayed on the surface at only one cycle. More Sol B deposition brought about more surface functionalized silica nanoparticles on the surface and smooth surface become more rough as the deposition cycle increases. The results indicate that by tuning the roughness of the surface, it can become ultra hydrophobic and further tuning of the roughness to optimum level, surface can exhibit superhydrophobic properties. This conclusion become more convincing when Sol B applied with 1 wt% silica, and only 3 cycles of spraying made the surface superhydrophobic with very low sliding angle and hysteresis. These results are further proof of the importance of surface roughness for the hydrophobicity. It is only by designing optimum surface roughness that a surface can change from hydrophobic to superhydrophobic state. Figure 21  showing the water droplet shape and corresponding static contact angle on the bare glass (uncoated glass substrate) and coated samples with 1.0 wt% silica nanoparticles.

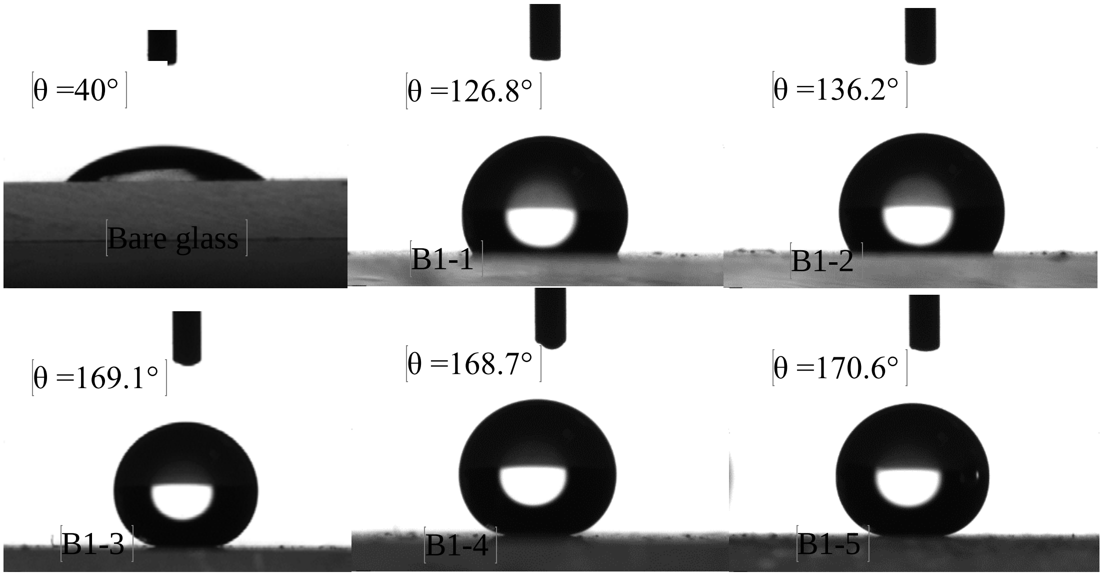

Figure 21 Water droplet on the samples and its contact angle.

Table 6 Static, sliding, advancing, and receding angles and hysteresis of the samples sprayed with Solution B including 1 wt% silica Nanoparticles.

| **Samples** | **CA** | **SA** | **AA** | **RA** | **H** |
|---|---|---|---|---|---|
| **B1-1** | 126.8±4.6 | 15.4±2.3 | 131.1±2.6 | 116.3±4.2 | 14.8±3.6 |
| **B1-2** | 136.2±4.8 | 23±4.5 | 141.8±5.8 | 113.9±7.7 | 27.9±4.7 |
| **B1-3** | 169.1±1.0 | 1±0 | 165.9±2.5 | 159.4±1.4 | 6.5±1.8 |
| **B1-4** | 168.7±2.8 | 1±0 | 166±1.4 | 160.4±2.9 | 5.5±2.5 |
| **B1-5** | 170.6±1.1 | 1±0 | 167.3±0.9 | 162.7±3.0 | 4.6±2.5 |

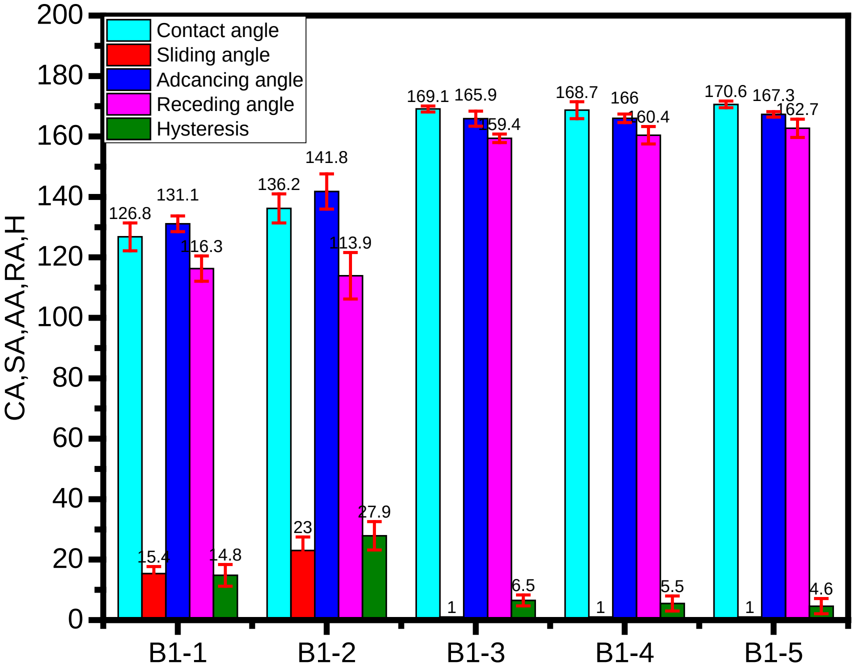

Figure 22 Contact angle, sliding angle, advancing angle, receding angle and hysteresis of the samples sprayed with Solution B including 1 wt% silica Nanoparticles.

Although higher number of spray cycles can result in higher static water contact angle and lower sliding angle and hysteresis as evident from the Figure 22, but more silica particles are deposited decreasing the transmittance of the surface. The effect of silica deposition on the transparency of such surfaces is discussed in the following sections.

Figure 23 shows a water droplet starting to move at a very low tilting angle. A very low sliding angle of water droplet on sample B1-3 approximately 1° indicates that the water droplet on this surface is in Cassie-Baxter state.

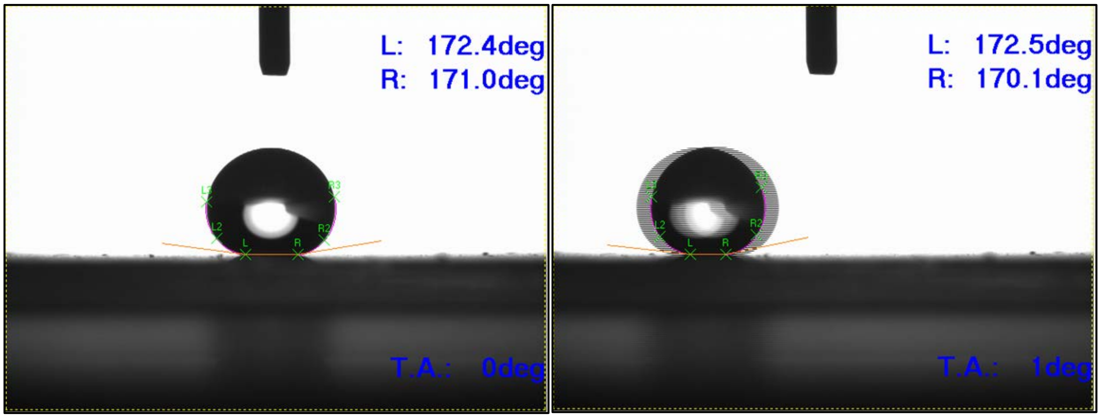

Figure 23 water droplet sliding on the surface of B1-3 sample after tilting at 1°.

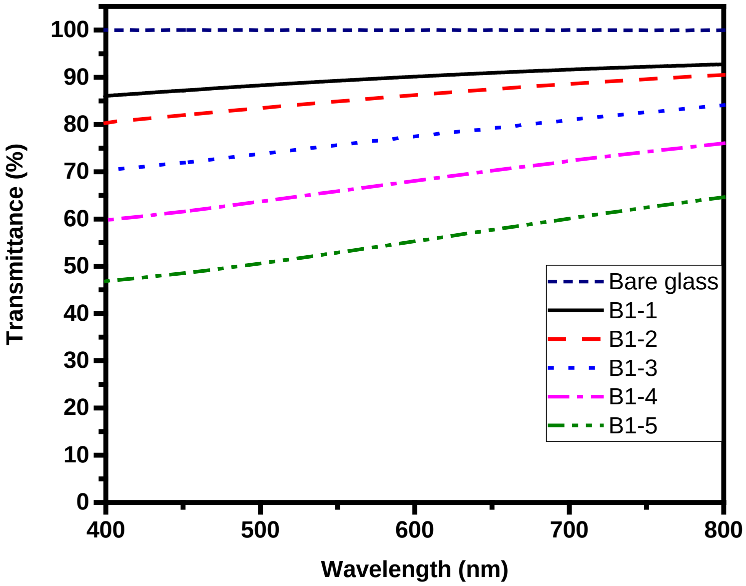

Figure 24 Transmittance of glass substrate coated with 1wt% silica nanoparticles.

Figure 24, it is clear that sample B1-3 is be the best sample with the optimum combination of superhydrophobicity and transmittance to visible light. It has a CA of 169.1°, SA of 1° and hysteresis of 6.5. Furthermore, it shows more than 70% transmittance at a wavelength of 400 nm. With an increase of visible light wavelength its transmittance also increased correspondingly and almost reached up to 85% at the wavelength of 800 nm as showed in the Figure 24. Figure 25 shows visual appearance of the uncoated glass and coated glass (sample B1-3).

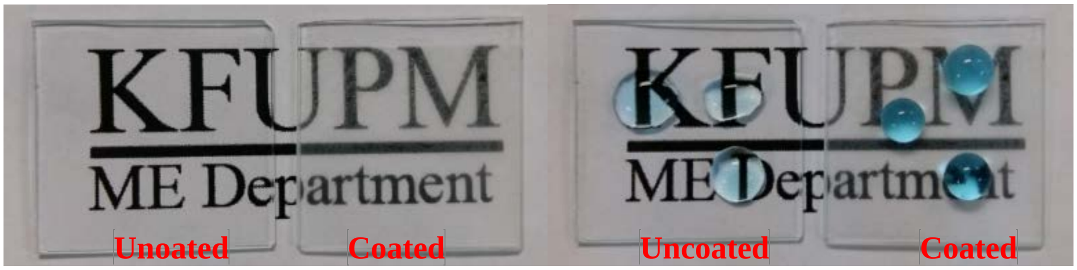

Figure 25 Visual appearance of uncoated glass and coated glass（B1-3 sample).

Table 7 and Figure 26 show that regardless of the number of cycles all samples sprayed with Sol B having 2.0 wt% silica nanoparticles result in superhydrophobic surface. Although Sol B with 2.0 wt% of silica nanoparticles sprayed only by one cycle (B2-1) can make the surface superhydrophobic, its transmittance is found to be far below that of B1-3.

Table 7 Contact angle, sliding angle, advancing angle, receding angle and hysteresis of the samples sprayed with solution B including 2 wt% silica Nanoparticles.

| **Samples** | **CA** | **SA** | **AA** | **RA** | **H** |
|---|---|---|---|---|---|
| **B2-1** | 173.2±2.8 | 1±0 | 170.4±1.8 | 167.5±1.2 | 3.2±1.9 |
| **B2-2** | 173.2±2.0 | 1±0 | 173±2.0 | 170.3±0.3 | 2.7±1.9 |
| **B2-3** | 172.7±1.7 | 1±0 | 170.7±3.1 | 165.9±4.6 | 4.7±2.9 |

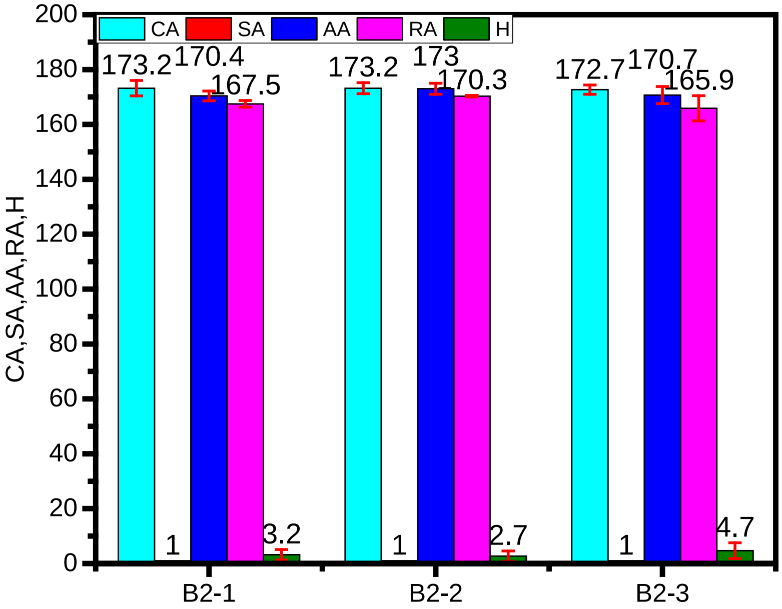

Figure 26 Water contact angle details of the samples sprayed with solution B including 2 wt% silica Nanoparticles.

## 4.3 Superhydrophobic surface morphology

### 4.3.1 Surface roughness

Roughness of the surface was measured by 3D optical profilometer. 2D, line scan and 3D surface topography shown below indicate that sample B1-1 havs higher roughness than the B1-3. For the sample B1-1, although deposition of Sol B is only one cycle, it has higher roughness than the sample B1-3. By observing the corresponding line scan of B1-1 it is easy to understand that the surface roughness is mainly due to the rough deposition of the first layer of Sol A by manual spray coating process. The first layer creates the roughness at micro level giving rise to roughness of the surface when it was measured on the area of 1.7×2.2mm. This is clearer when the line scans of two samples are compared. On sample B1-3 line scan we can observe its waviness and small spikes deviated from waviness, creating sub-micron and nano-roughness more uniformly. Although the roughness of the surface can be measured on large area by 3D optical profilometer, but it may not give the actual roughness value of the surface at micro and nano level like Atomic Force Microscopy. Another reason for this, is that the optical profilometer collects the surface information by reflected light. Hence, if light passes through a transparent surface, the results may be misleading. Although in our case the samples used to measure the surface roughness were coated with gold to minimize the error between readings from optical profilometer and actual roughness. Although sample B1-1 has higher roughness, but lacks the dual scale roughness structure like B1-3, that is crucial for the extreme water-repellencey. It is clear from the line scan of these two samples that sample B1-3 has the dual scale combination of nano and micro structure which is preferred for non-wetting characteristics.

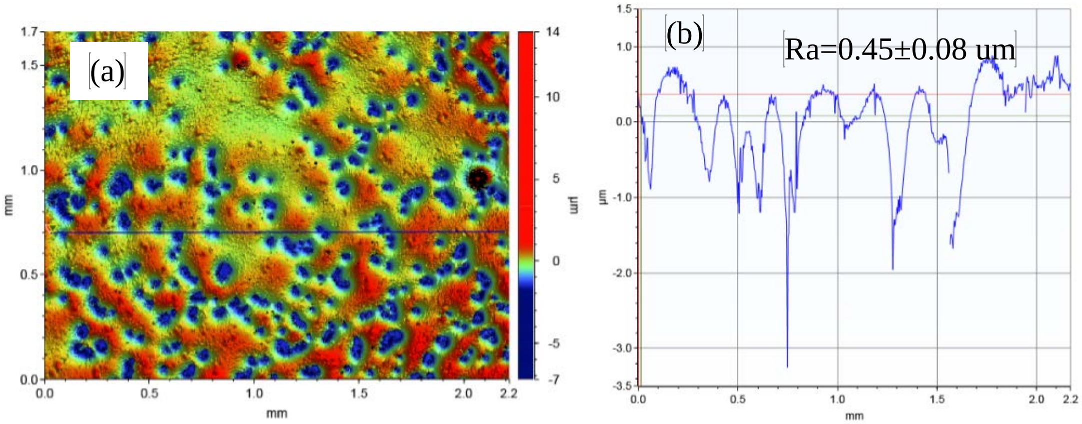

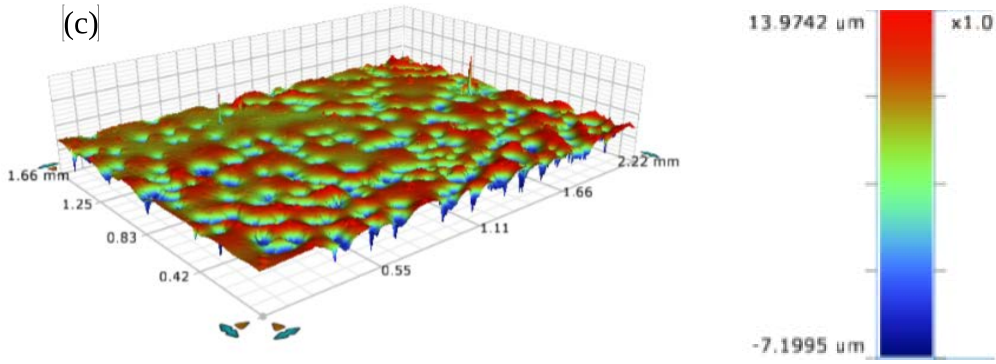

Figure 27 Optical images of B1-1sample from (a) 2-D, (b) Line scan and (c) 3-D view of surface morphology.

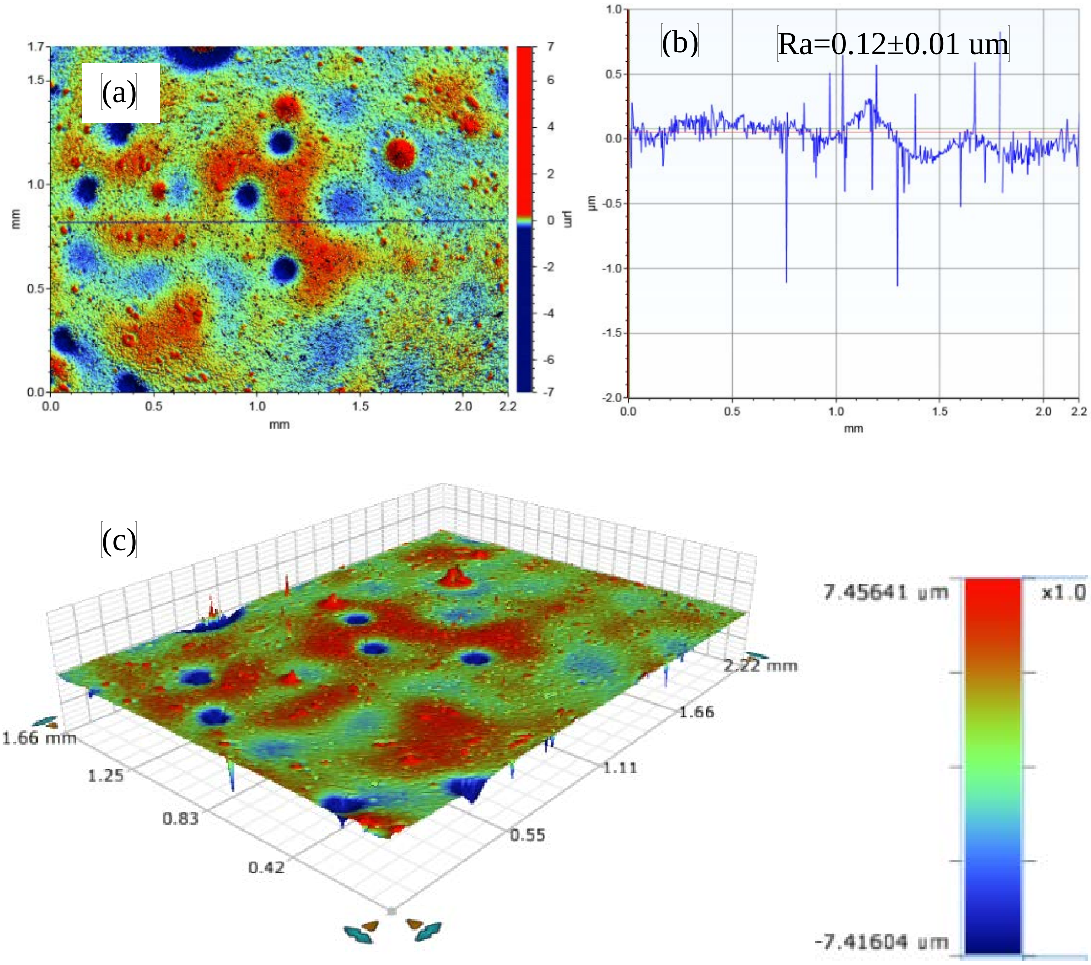

Figure 28 Optical images of B1-3 sample from (a) 2-D, (b) Line scan and (c) 3-D view of surface morphology.

### 4.3.2 SEM, XPS, and Raman Analyses

Figure 29 and Figure 31 show SEM images of sample B1-1 and B1-3 at different magnifications, respectively.

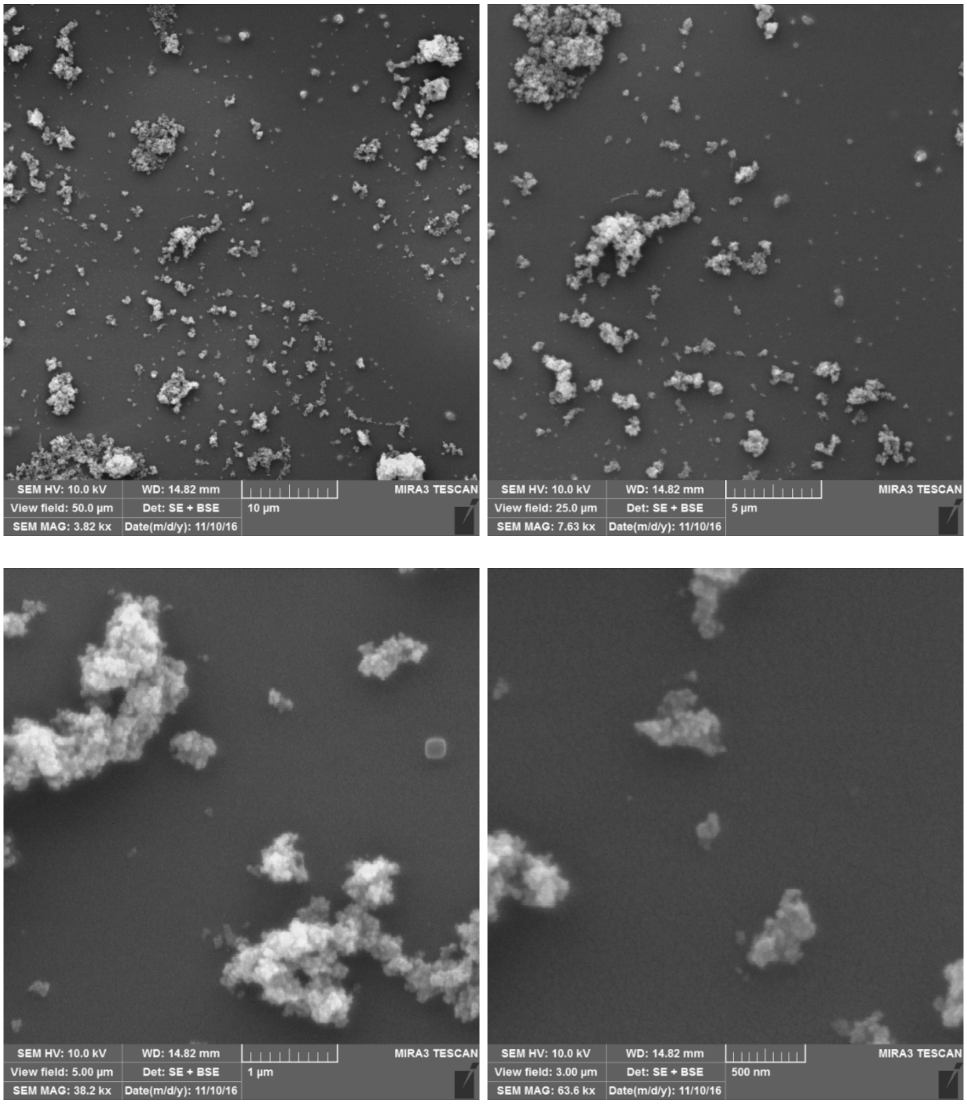

Figure 29 SEM images of B1-1sample at different magnifications

The SEM images of sample B1-1 from different magnifications, show clearly that some of the area is not fully covered by the silica nanoparticles, for this reason, the surface roughness created by the particles is not enough to create air pockets for resulting hydrophobicity. It is clear from the CA result that hydrophobic surface on the sample B1-1 resulted from the low surface energy rather than the roughness since the sample B0-1 (sprayed with 0 wt%) having hydrophobic surface and CA result almost near to the sample B1-1. According to the chemicals (such as PFOTS) we used in our experiment and from literature statement that closest hexagonal packing of $CF_3$ groups gives the lowest surface energy of the materials. As the surface of samples were sprayed with PFOTS and they may have surface energy as low as 6 $mJ/m^2$ [44–46].

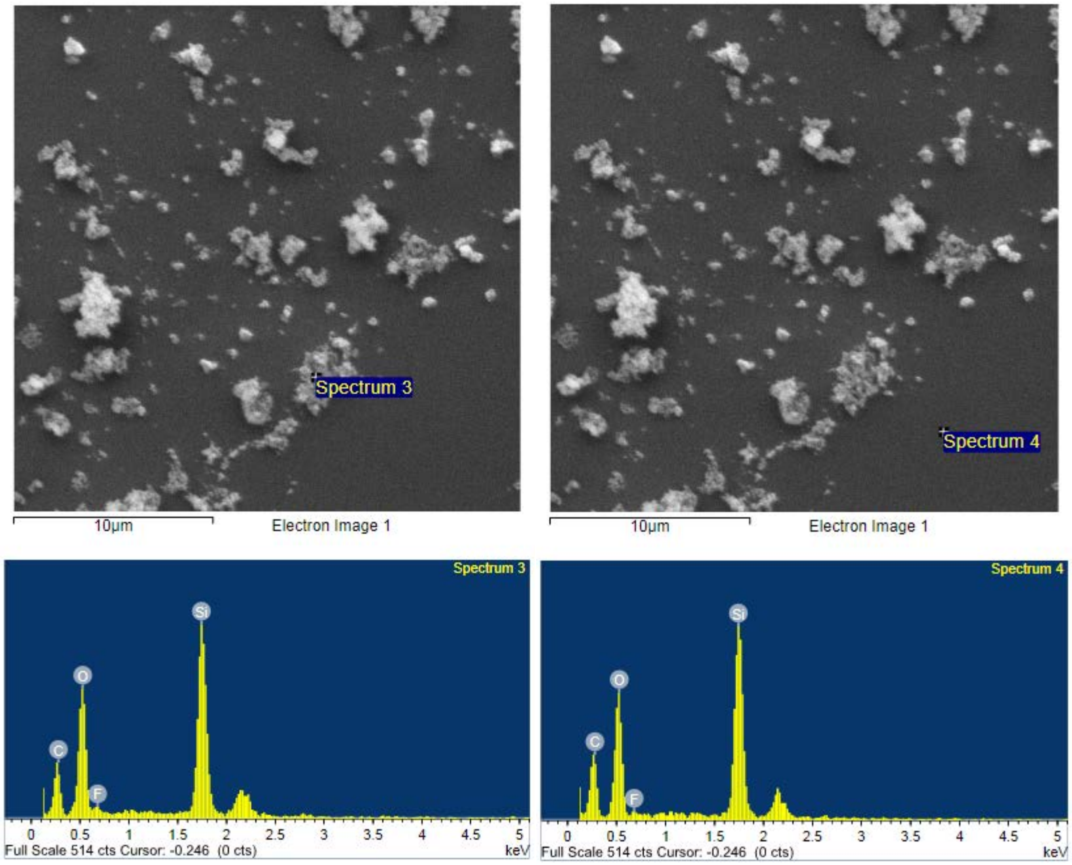

Figure 30 EDS analysis of B1-1sample at different spot.

When the SEM image of sample B1-1 and B1-3 are compared, it is observed that the surface of the sample B1-3 is better covered by the silica nanoparticles, in addition to that the agglomeration of silica particles is aslo observed. Agglomeration of the silica particles at micron or submicron level can be advantageous in creating micro and nano-roughness structure [47–49].

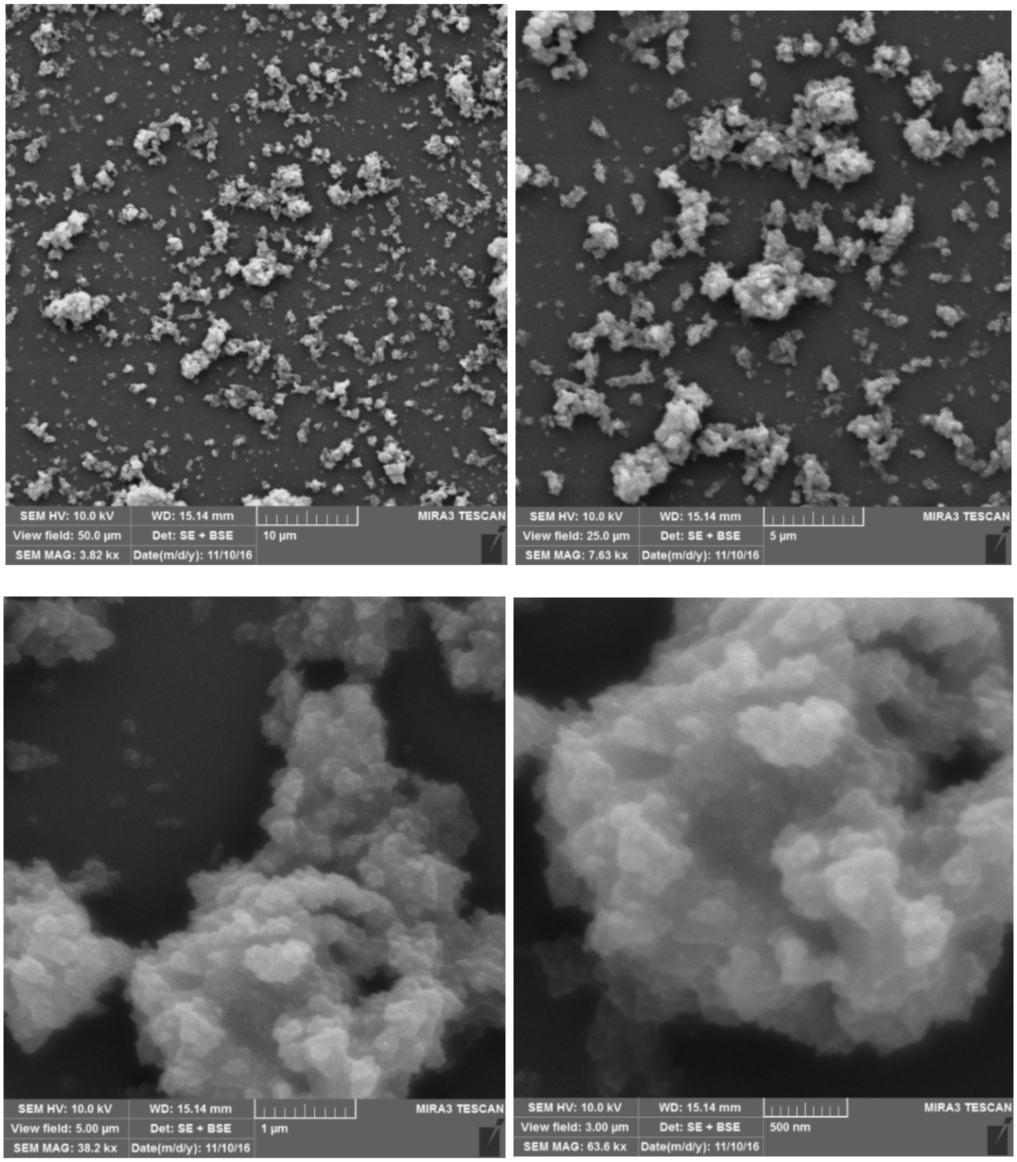

Figure 31 SEM images of B1-3sample at different magnifications

Figure 30 and Figure 32 are EDS elemental analysis of samples B1-1 and B1-3, respectively. EDS results from both samples did not observe the EDS peak of Cl, indicating that hydrolyzation and condensation of PFOTS took place completely. First -Cl replaced by the -OH groups by hydrolyzation reaction followed by the condensation reaction between two Si-OH groups to for siloxane (Si-O-Si) network. Presence of Fe peak in EDS spectrum may be due to 99.5% trace metals basis of silica nanoparticles used.

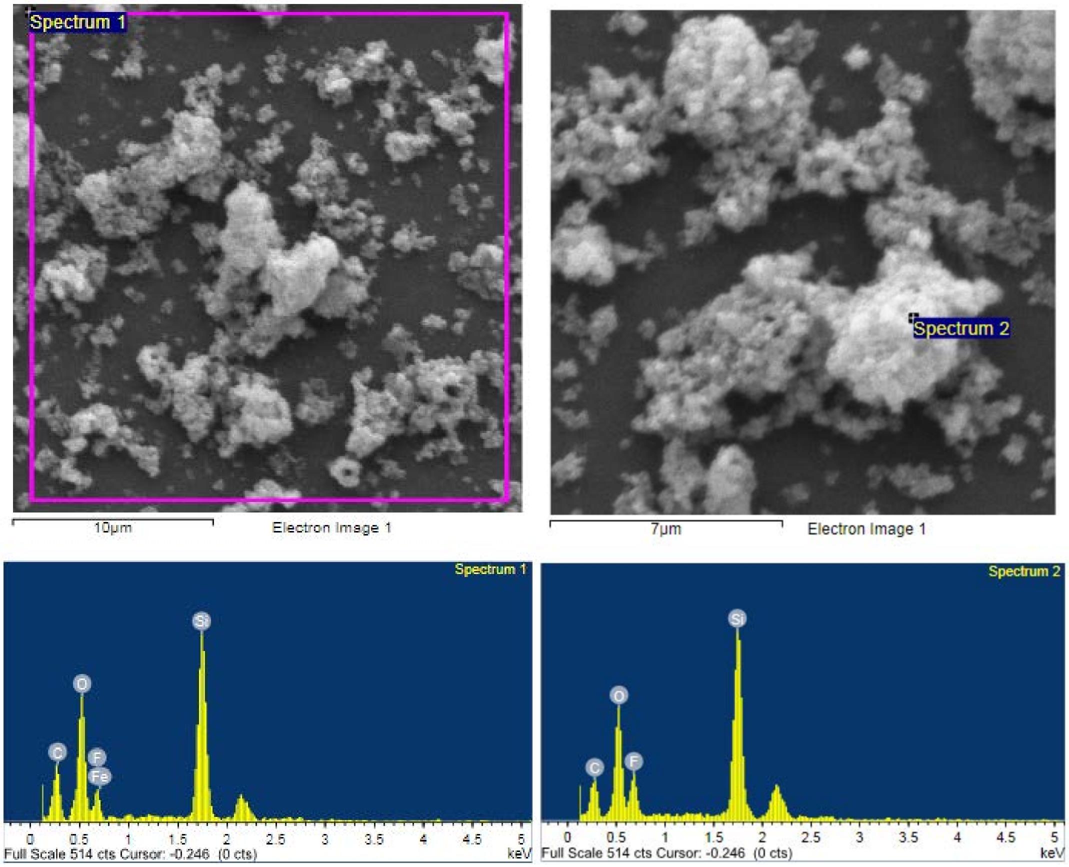

Figure 32 EDS analysis of B1-3sample at different spot.

The chemical composition and surface atomic concentration of sample B1-3 was further characterized by XPS, as shown in Figure 33, the C (C1s 284 eV, CKLL 982 eV) and

O1s (532 eV) peaks can be seen clearly in the spectrum. Si (Si2p 102 eV and Si2s 153 eV) and F (F1s 688 eV and FKLL 835 eV) signals, characteristic of covalently bonded Si and F, was detected. High-resolution XPS provides additional insight into the chemical composition of the film further and confirming the presence of $CF_2$ and $CF_3$ groups [50]. Missing of Cl2p (200 eV) peak from the spectra indicating that the Cl atoms on the PFOTS completely replaced by OH groups and via condensation reaction connected to the silica particles as well as first layer and further confirming the conclusion from the EDS result.

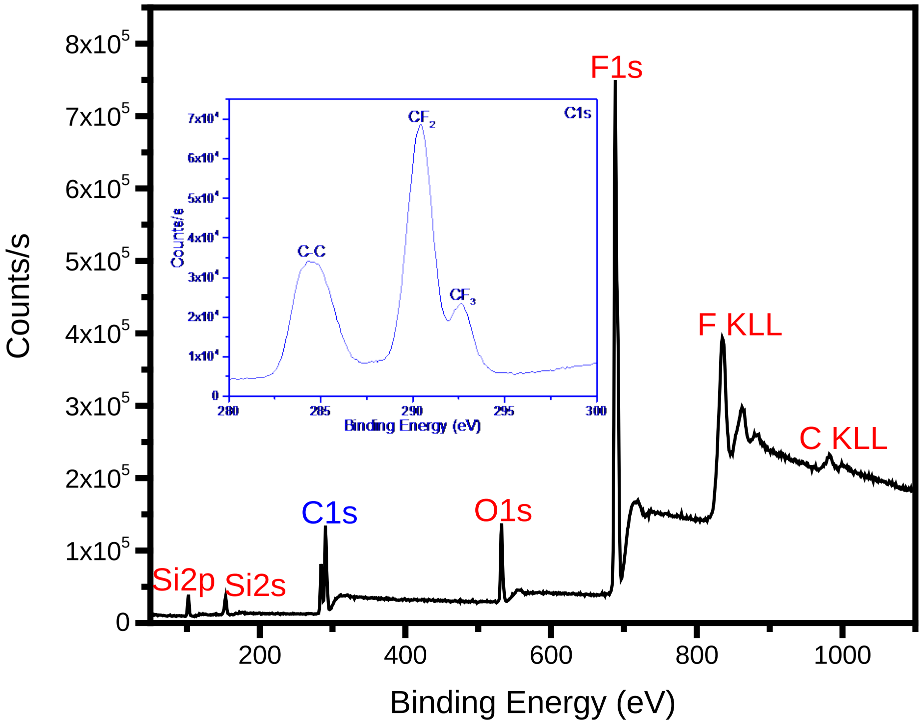

Figure 33 XPS spectra of sample B1-3.

Selected sample B1-1 and B1-3 were further characterized by Raman Spectroscopy, Figure 34 shows the labeled peak positions and Table 8 provides summarized Raman bands assignment of corresponding peaks.

Table 8 Raman bands assignment [51]–[53].

| **Raman bands (cm-1)** | **Assignment** |
|---|---|
| 3056 | epoxy group CH stretching |
| 3003 | epoxy group CH stretching |
| 2970 | Anti-symmetric stretching vibrations of $CH_3$ |
| 2908 | Anti-symmetric stretching vibrations of $CH_3$ |
| 1482 | $CH_3$ $\delta_s$ |
| 1457 | $CH_3$ $\delta_a$ |
| 1413 | epoxy group |
| 1256 | epoxy ring breathing |
| 1131 | epoxy group |
| 570 | $CF_3$ symmetric deformation |
| 480 | Si-O-Si |
| 356 | $CF_2$ twisting |

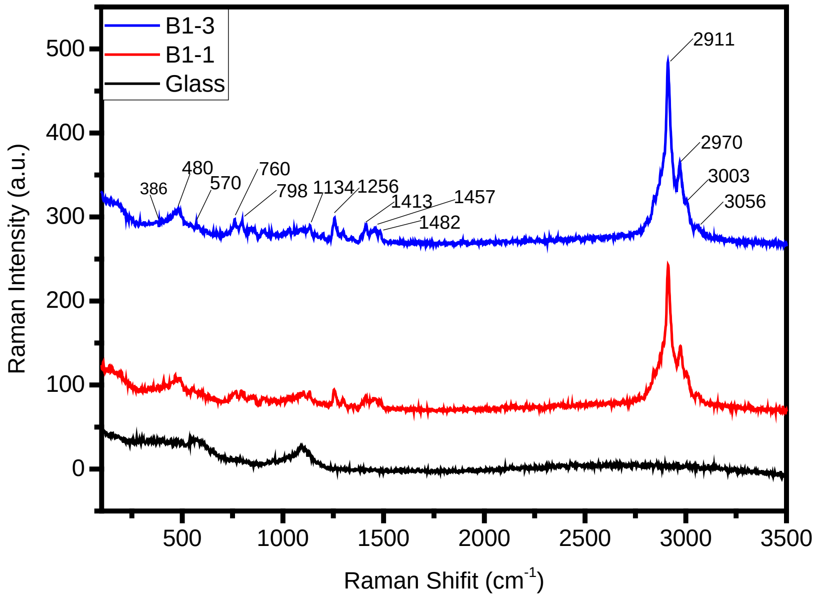

Figure 34 Raman spectroscopy of Sample B1-1 and B1-3.

Both sample B1-1 and B1-3 having similar Raman spectra with only difference in peak intensity. For both samples, presence of the $CF_2$, $CF_3$ peaks indicates that took place successfull functionalization of the silica nanoparticles surface by the PFOTS, other peaks contributed from the first layer which is formed from hydrolysis and condensation of MTMS and GLYMO. There is almost no small difference between B1-1 and B1-3 spectra peaks position, as B1-1 and B1-3 samples are both coated with second layer Sol B, only with difference in spray cycles. Although both B1-1 and B1-3 having same surface chemistry but showing different wettability to the water droplets. B1-3 showed less wettability than the B1-1. This difference in wettability indicates that the importance of surface roughness with the combination of micro and nano features are essential for the surface change from hydrophobic to superhydrophbic [54–56]. As shown in Figure 31, SEM images B1-3 sample surface deposited with more silica particles, and surface thus is provided with enough roughness that necessary to create superhydrophobic surface. Also, agglomeration of the silica nanoparticles at some extent is favorable for superhydrophobicity since it can provide surface with hierarchical structure of micro-nano roughness.

## 4.4 Self-cleaning properties

Figure 35 illustrates self-cleaning mechanism that superhydrophobic surfaces are expected to undergo. When a surface is superhydrophobic, it is not easily wetted by water. When water droplets hit the superhydrophobic surface, they will bounce away and/or start rolling down from the surface. During the rolling, water droplets can collect certain amounts of dust particles.

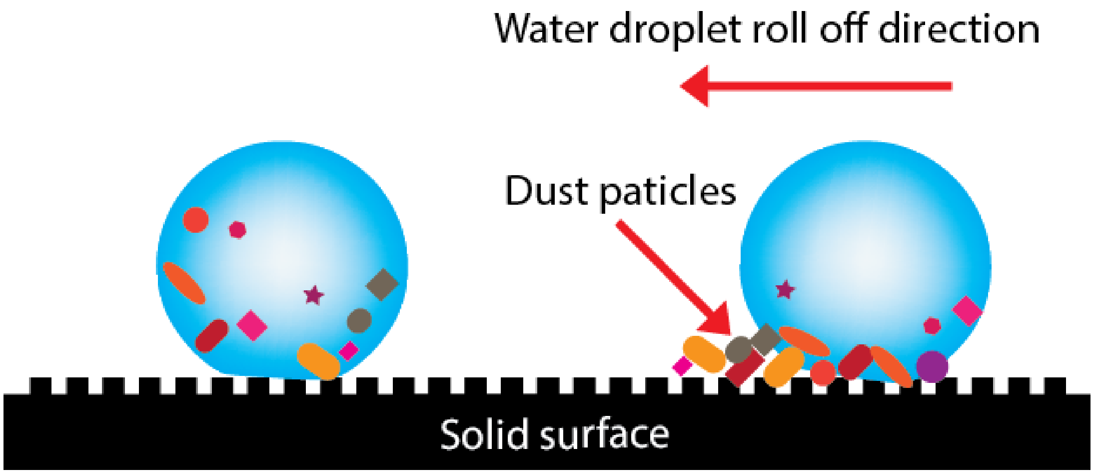

Figure 35 Self-cleaning mechanism of superhydrophobic surface.

Figure 36 shows how this mechanism works on the surface of B1-3 sample. It compares the self-cleaning ability of both coated and bare glass when tilted around with the angle of 10°. The adjacent surfaces are covered with a similar amount of sand particles. The droplets of colored water are shown to roll off the coated surface taking away the dust, while those on the bare surface sticked to it. It is worth mentioning that only 6 droplets of water were sufficient to remove all the dust on the 25×25 mm area of coated glass surface.

As water droplet spread on the hydrophilic surface, not like superhydrophobic surface, dust particles not removed by water droplets. The mud formed, from dust particles in humid air condition, on the surface of glass more strongly adhered to surface. Once mud dried, there is formation of a thin mud solution film [57] between dust particles and glass surface and alters the surface characteristics.

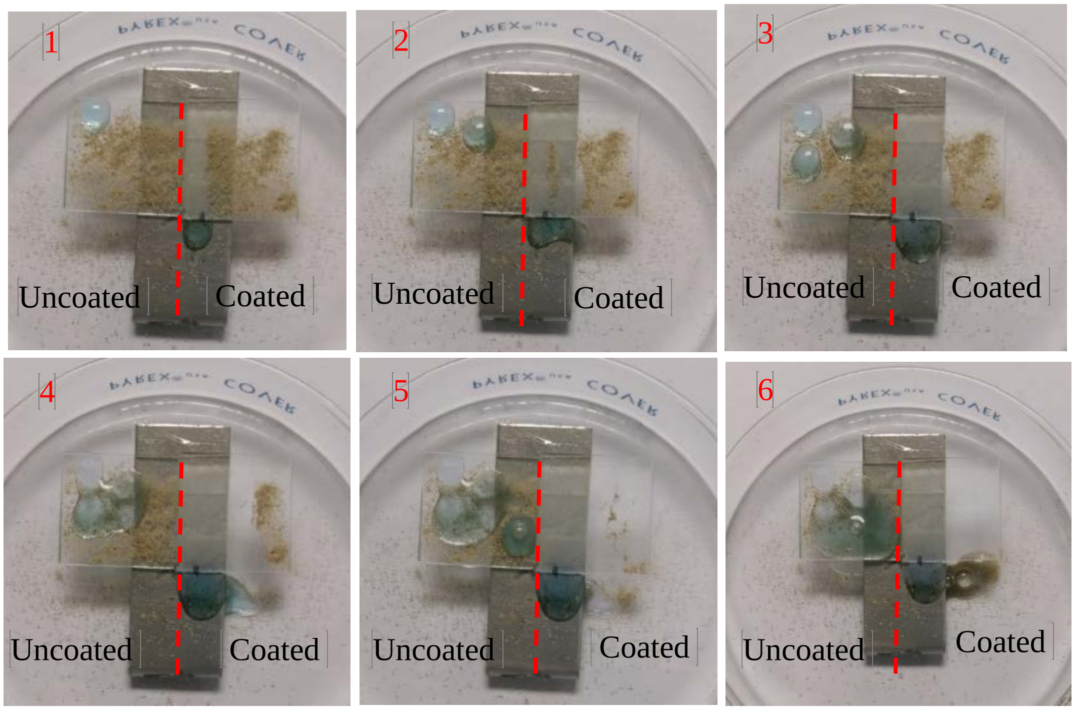

Figure 36 Comparison of self-cleaning effect of the coated glass and bare glass

## 4.5 Thermal stability and effect of annealing

Sample B1-3, having shown to have optimum properties in terms of superhydrophobicity and transmittance, was selected for testing the thermal stability of the superhydrophobic coating. To do so, the sample was kept in the furnace for 2 hours at 300°C, 350°C and 400°C, then the different contact angles and hysteresis were measured to study the thermal stability of coatings on glass substrate. The results, illustrated in table 5 reveal that annealing at temperatures higher than 300°C for two hours drastically reduces the contact angle.

Table 5 Contact angle, sliding angle, advancing angle, receding angle and hysteresis of the sample B1-3 annealed at different temperature.

| Temperature | CA | SA | AA(L) | RA(R) | Hysteresis (H) |
|---|---|---|---|---|---|
| **0°C** | 169.1±1.0 | 1±0 | 165.9±2.5 | 159.4±1.4 | 6.5±1.8 |
| **300°C** | 167.1±1.0 | 1±0 | 166.2±2.7 | 159.3±1.6 | 6.9±2.1 |
| **350°C** | 137.5±3.8 | NA | NA | NA | NA |
| **400°C** | 72.1±6.4 | NA | NA | NA | NA |

Figure 26 shows that annealing improved the overall transmittance of the surface by about 8%. Similar results were reported by other researchers [58]–[60]. Budunoglu et al [7] reported that optical transparency can be further improved when some films are calcinated under an appropriate temperature resulting in even higher optical transmission than the bare glass slide because of the reduced back reflection. Superhydrophobic surface can be oxidized at elevated temperature resulting to loss of hydrophobicity as it is evident from the results of our study obtained at 400 °C.

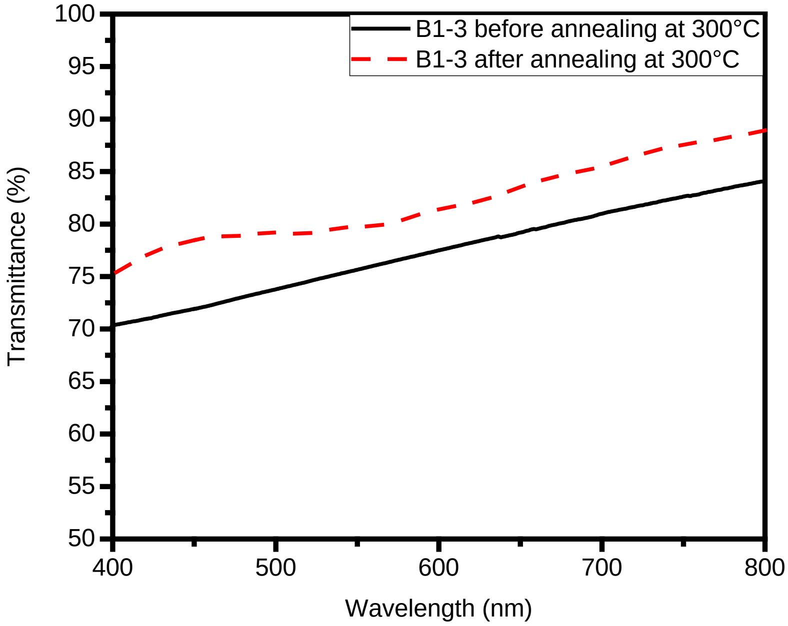

Figure 37 Transmittance of sample B1-3 before and after annealing at 300 °C.

Degradation of the superhydrophobic surface is mainly due to a decomposition and oxidation of surface chemistry rather than to a change in the surface roughness [61]. FTIR analysis of the surface before and after heat treatment at different temperatures indicated that hydrocarbon absorptions were absent. Figure 38 illustrates FTIR bands peak position for room temperature (RT) and heat-treated samples.

The FTIR spectroscopy bands occurred at 1005 cm$^{-1}$ and 1061cm$^{-1}$ corresponding to Si-O-Si stretching [62], [63]. Two tiny peaks at 1235 cm$^{-1}$ and 1196 cm$^{-1}$ superimposed between 1061 and 1260 cm$^{-1}$ on the left shoulder of the Si–O–Si peak at 1061 cm$^{-1}$ are due to the stretching vibration of C–F bonds anticipated, which is the sign of the fluorination of the silica nanoparticles by the PFOTS molecules [64], [65]. However, these two tiny peaks become less significant on the 300ºC line and totally disappear on the 350ºC and 400ºC lines. Without the presence of low surface energy functional groups such as $CF_2$ and $CF_3$, the surface water contact angle decreased to 137.5° for the sample heat treated at 350°C and to 72.1° for the sample heat treated at 400°C. Peak around 907 cm$^{-1}$ corresponding to C–H bonds arising from PFOTS molecules [66] is not present on the lines of heat treated samples.

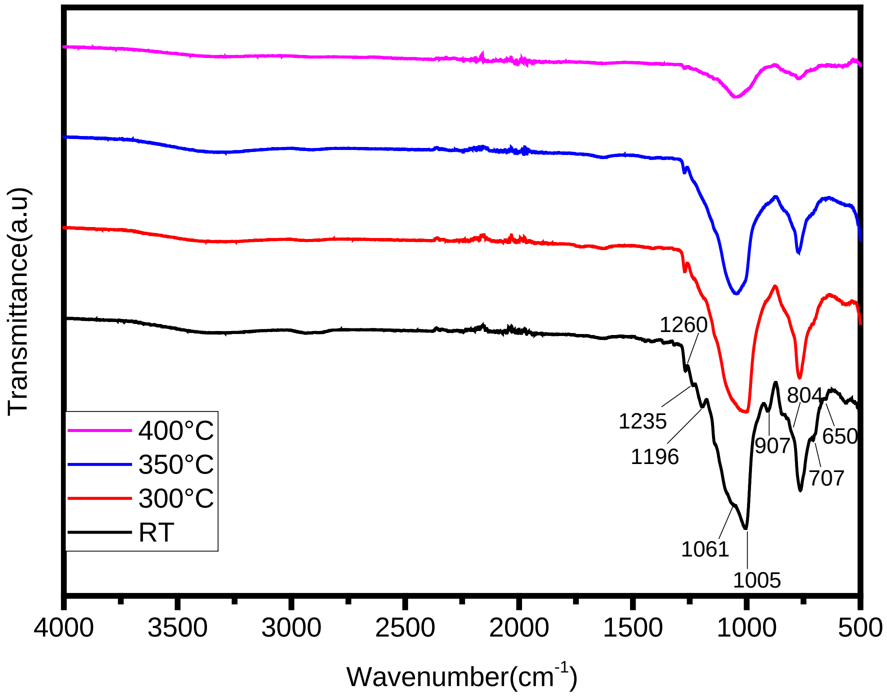

Figure 38 FTIR spectra after annealed at different temperature.

The existence of C–F bonds in the form of $CF_2$ and $CF_3$ are also located at 650 and 707 $cm^{-1}$ [67], [68]. These functional groups, which are responsible for lowering the surface energy, become less significant on the 300 ºC and totally disappear at higher temperatures. The absence of these peaks on the samples heat-treated at 350 ºC and 400 ºC result in drastic reduction of the water contact angles and in increasing the sliding angle and hysteresis. The FTIR spectroscopy bands at 1260 $cm^{-1}$ ($CH_3$ bending) and 804 $cm^{-1}$ ($CH_3$ rocking) [51] which are present only on the RT, 300 ºC and 350 ºC lines indicate that 400 °C heat treatment has totally degraded the superhydrophobic surface. Although $CF_2$ and $CF_3$ peaks were absent on the 350 ºC lines, the presence of $CH_3$ peaks still give this sample some hydrophobic characteristics as reported earlier. As stated in the literature review, $CF_2$ and $CF_3$ groups have lowest surface energy compared to the

$CH_3$ and other functional ending groups. This explains why the sample heat treated at 350 ºC is still hydrophobic when surface maintains proper roughness. This is a further indication that the combination of optimum surface roughness and low surface chemistry are vital for the fabrication of the superhydrophobic surfaces. All the FTIR bands peaks position and assigned functional groups were tabulated in the Table 9 below.

Table 9 Fourier transform infrared bands assignment.

| **FTIR bands ($cm^{-1}$)** | **Assignment** |
|---|---|
| 1235 | stretching vibration of C–F bonds |
| 1196 | stretching vibration of C–F bonds |
| 1260 | $CH_3$ bending |
| 803 | $CH_3$ rocking |
| 1005 | Si-O-Si stretching |
| 1061 | Si-O-Si stretching |
| 907 | C–H bonds (arising from PFOTS molecules) |
| 650 | $CF_2$ and $CF_3$ |
| 707 | $CF_2$ and $CF_3$ |

## 4.6 Resistance to ultraviolet irradiation

After the long period of UV irradiation (10 hours at UV lamp intensity of 2500 $W/m^2$ and 2 hours at UV lamp intensity of 30000 $W/m^2$), test sample contact angle details are measured and are reported in compare to C-C bond (bond energy of 346 kJ/mol) [61].

Table 10. According to the literature [69], long-term daily mean values of sunshine duration and Global Solar Radiation (GSR) is about 9.2 hours and 5123 $W/m^2$ per day respectively in the region of Riyadh, Saudi Arabia (Lat. is 24.57°, Lon. is 46.72°, and Alt. is 564 m). Approximately 5% of solar terrestrial radiation is Ultra-Violet Radiation

(UVR) (approximately 256 W/m$^2$ per day). In our study, the highest intensity of the UV lamp 100 times more than the actual UV light intensity in the Riyadh region. The results show that the average values for the different types of angles are almost identical before and after UV irradiation. This is an indication of high UV resistance of the produced superhydophobic surface. This is mainly due to the presence of Si-O-Si (Si-O bond energy of 452 kJ/mol) and C-F (bond energy of 485 kJ/mol) high chemical energy bonding which require very high energy or very long exposure time to degrade compare to C-C bond (bond energy of 346 kJ/mol) [61].

Table 10 Contact angle, sliding angle, advancing angle, receding angle and hysteresis of sample B1-3 before and after ultraviolet irradiation test.

| **UV testing** | **CA** | **SA** | **Advancing contact angle (AA)** | **Receding contact angle (RA)** | **Hysteresis (H)** |
|---|---|---|---|---|---|
| **Before** | 169.1±1.0 | 1±0 | 165.9±2.5 | 159.4±1.4 | 6.5±1.8 |
| **After** | 169.0±1.2 | 1±0 | 166.0±2.2 | 159.1±1.3 | 6.9±1.9 |

From Figure 39, it can be clearly observed that the A4 white paper placed under the sample (dashed circle line area) changed to yellowish color after UV irradiation test. The dashed circle area is approximately the spot size of UV light when irradiated on the surface of sample. It is also clear from Figure 39, that not only has the surface retained its hydrophobicity, it has also maintained its transparency.

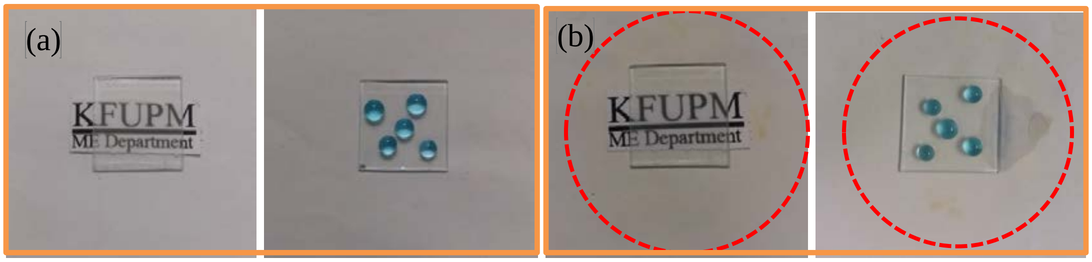

Figure 39 Hydrophobicity and transmittance of B1-3 surface (a) before and (b) after UV exposure.

For the silica film, only small side groups (such as PFOTS molecules, connencted to silica surface by condensation reaction) exist on the surface; these moieties are more UV stable than are polymers because negligible impurities and less UV-fragile defects exist on the silica surface. Thus, the silica film exhibits better UV stability than do organic polymers. In addition, the silica main chain is comprised of Si–O bonds, which have higher bond strength and thus better UV stability than organic polymer materials [61]. The above proven UV irradiation resistance enables the application of the fabricated superhydrophobic surface outdoor field environment.

Basically, organic polymers with reactive (e.g., double bonds) or low energy (e.g., tertiary hydrogen) structures in the polymer main chain, are vulnerable to UV irradiation. When impurities (i.e., catalyst) and UV absorbing groups are present, the polymer can undergo a photo-oxidation process to form carbonyl or hydroxyl groups on the surface and thus degrade (unzip) into smaller chains [26].

## 4.7 Superhydrophobic surface resistance to water jet

Table 11 and Figure 40 show the measured angles before and after water jet that characterize the hydrophobicity of the surface. A comparison of the contact angle details before and after one hour of water jet testing is also shown in both the table and graph. It is evident that, the average values of static water contact angle, sliding angle and hysteresis did not experience any significant changes. This indicates that the intense water jet test did not damage the hydrophobicity of the surface by either removing silica nanoparticles on the surface or degrading the functional -$CF_3$ groups or other low surface energy functional groups. Without degradation of the surface chemistry and roughness of superhydrophobic surface, it can maintain same superhydrophobic properties after the water jet test. Minute change in the angles after test can be ascribed to the normal experimental measurement error.

Table 11 Contact angle details before and after water jet test.

| Water jet test | CA | SA | AA (L) | RA(R) | Hysteresis (H) |
|---|---|---|---|---|---|
| **Before** | 169.1±1.0 | 1±0 | 165.9±2.5 | 159.4±1.4 | 6.5±1.8 |
| **After** | 168.8±1.3 | 1±0 | 165.5±2.7 | 159.8±1.6 | 5.7±2.3 |

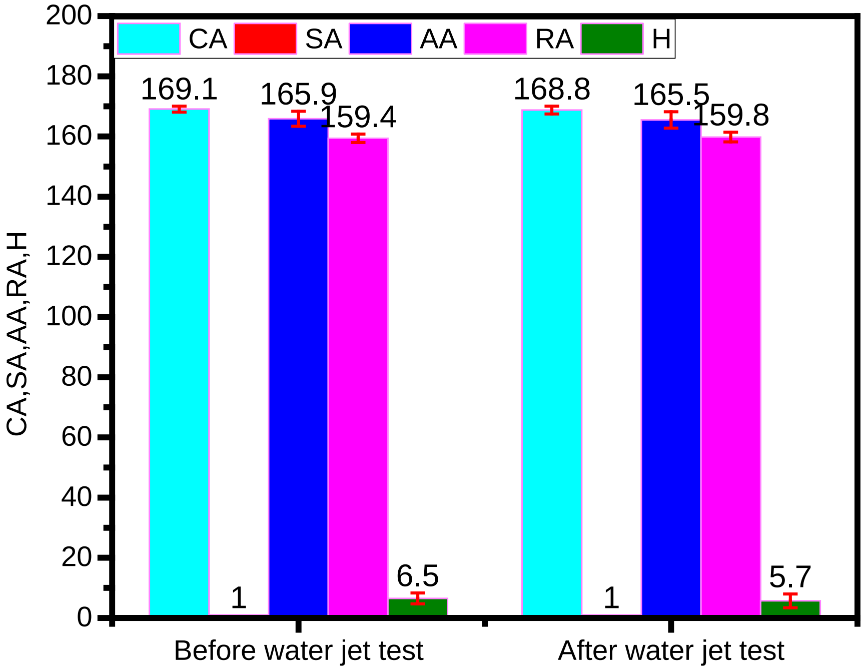

Figure 40 Contact angle details before and after water jet test.

## 4.8 Superhydrophobic surface resistance to abrasion

The results in Table 12 and Figure 42 describe the effect of abrasion on the hydrophobic properties of the fabricated surface after each cycle. It is clear that degradation of these properties becomes significant after few cycles. The abrasive surface of the sand paper has started to affect the roughness of the produced surface after the 1st cycle by flattening or removing its asperities as illustrated in Figure 41. It is worth mentioning that the static contact angle, CA, remains above 150°even after 5 cycles, but RA and H have been chiefly affected.

Figure 41 Effect of abrasion on superhydrophobic surface.

Table 12 Change in contact angles with number of cycles.

| No. of cycles | CA | SA | Advancing angle (AA) | Receding Angle (Ra) | Hysteresis(H) |
|---|---|---|---|---|---|
| **1 cycle** | 167.6±3.5 | 2.4±1.1 | 171±2.2 | 165.4±2.9 | 5.6±2.6 |
| **2 cycles** | 163.3±3.0 | 5.4±2.5 | 167.4±3.2 | 154.9±4.1 | 12.5±3.3 |
| **3 cycles** | 155.8±4.9 | 9.6±3.4 | 157.9±9.4 | 145.5±12.9 | 12.4±4.0 |
| **4 cycles** | 152.7±3.6 | 13.8±3.4 | 155.1±4.1 | 140.5±3.7 | 14.6±1.6 |
| **5 cycles** | 150.5±8 | 18.2±5.1 | 151.6±7.0 | 127.0±8.4 | 24.6±1.7 |

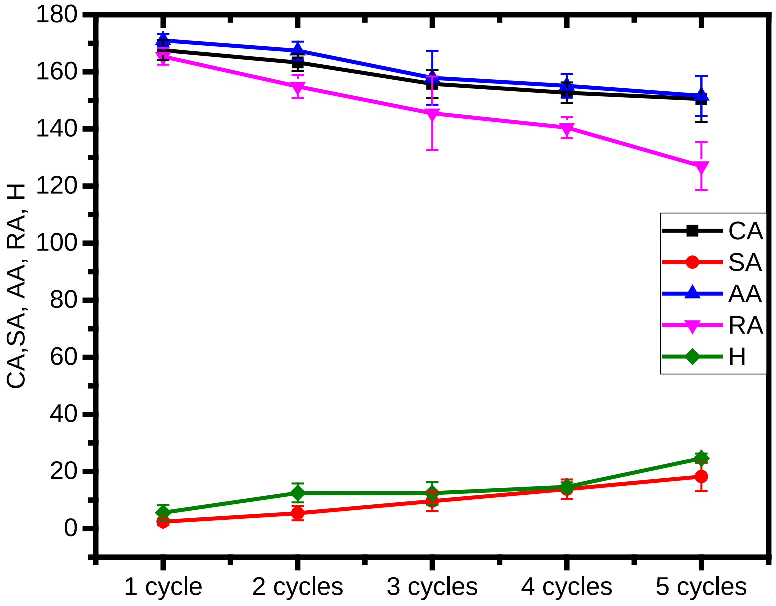

Figure 42 Change in contact angles as number of cycles.

## 4.9 Superhydrophobic surface resistance to sand blasting

Sand blasting test is one of the simulated tests that have been conducted to evaluate the robustness of the fabricated superhydophobic surface. This test can simulate the surface encountering outdoor aggressive weather conditions such as strong winds associated with sand storms, as is the case in desert areas. With the help of high-speed wind, sand particles may impinge on the surface with high potential energy . Sand blasting is considered as a very aggressive test and thus the coating on the central area of sample B1-3 was removed and only the edge areas were found to have a water contact angle of about 120°, as shown in Figure 43. After sand blasting, sample center becomes hydrophilic due to the removal of the coating by high speed sand particles, while the area on the edge remains still hydrophobic and water still can roll off the surface rather than spread on it.

Figure 43 After sand blasting sample center is hydrophilic and edge area still hydrophobic.

## 4.10 Application of developed solutions to different substrates

Figure 44 shows that once the optimized solutions (sol A and sol B) are developed, the resulting coating can be applied successfully to any substrate, making it superhydrophobic.

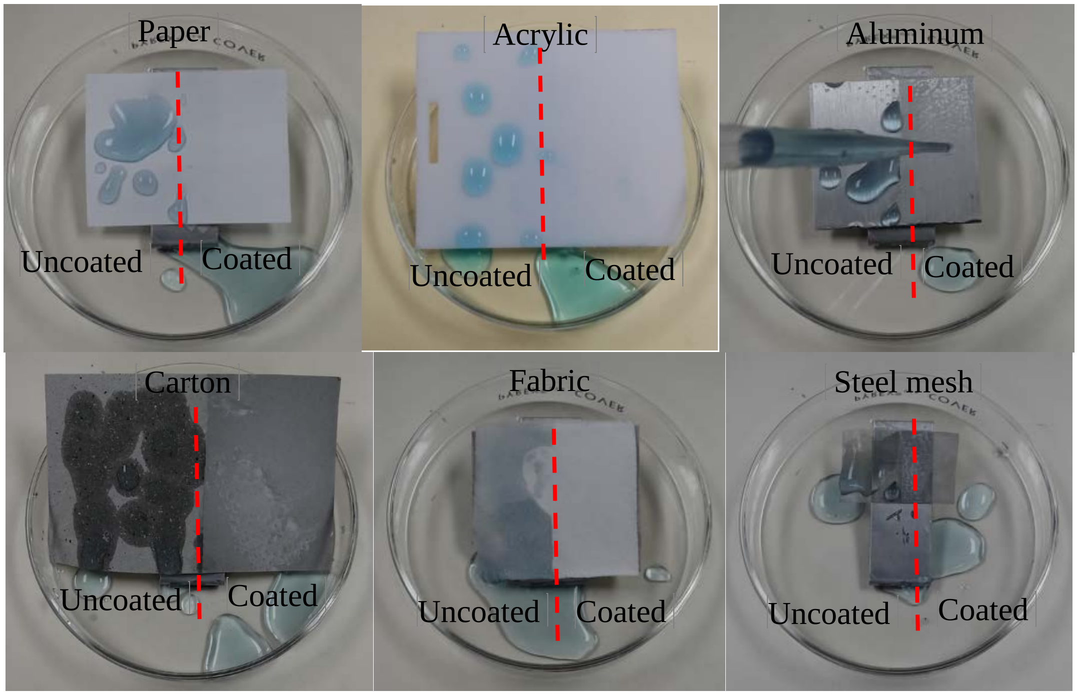

Figure 44 Application of solution on different substrates.

Paper, acrylic sheet, aluminum, carton, fabric cloth and steel mesh half were coated first with sol A and followed by sol B as explained in methodology part. It is clear from the Figure 44 that, all of the selected substrates were showing superhydrophobic nature after treatment. The developed coating solutions in this research can be applied to various substrates mainly because of first layer behaves as adhesive layer and/or binder. After functionalized silica particles are sprayed on the surface, particles can embed or stably bind to the first layer. It is worth to mention that very few coatings have shown success on a variety of substrates.

To see how water droplets, interact with the fabricated superhydrophobic surfaces and hydrophilic (uncoated) surface, water droplet motion was recorded by camera. A water droplet of about 7 μl and was dropped from a height of 10 cm on different coated and uncoated substrates such as paper, cloth (fabric), Aluminum sheet, glass, acrylic sheet, steel mesh. Figure 45 shows time-lapse photographs of how water droplets behave on the coated and uncoated surfaces of these materials. It is clear from the images that usually on coated superhydrophobic surfaces water droplets are bouncing. Leading to the conclusion that the developed coating is suitable for use in different applications, not only for PV panels.

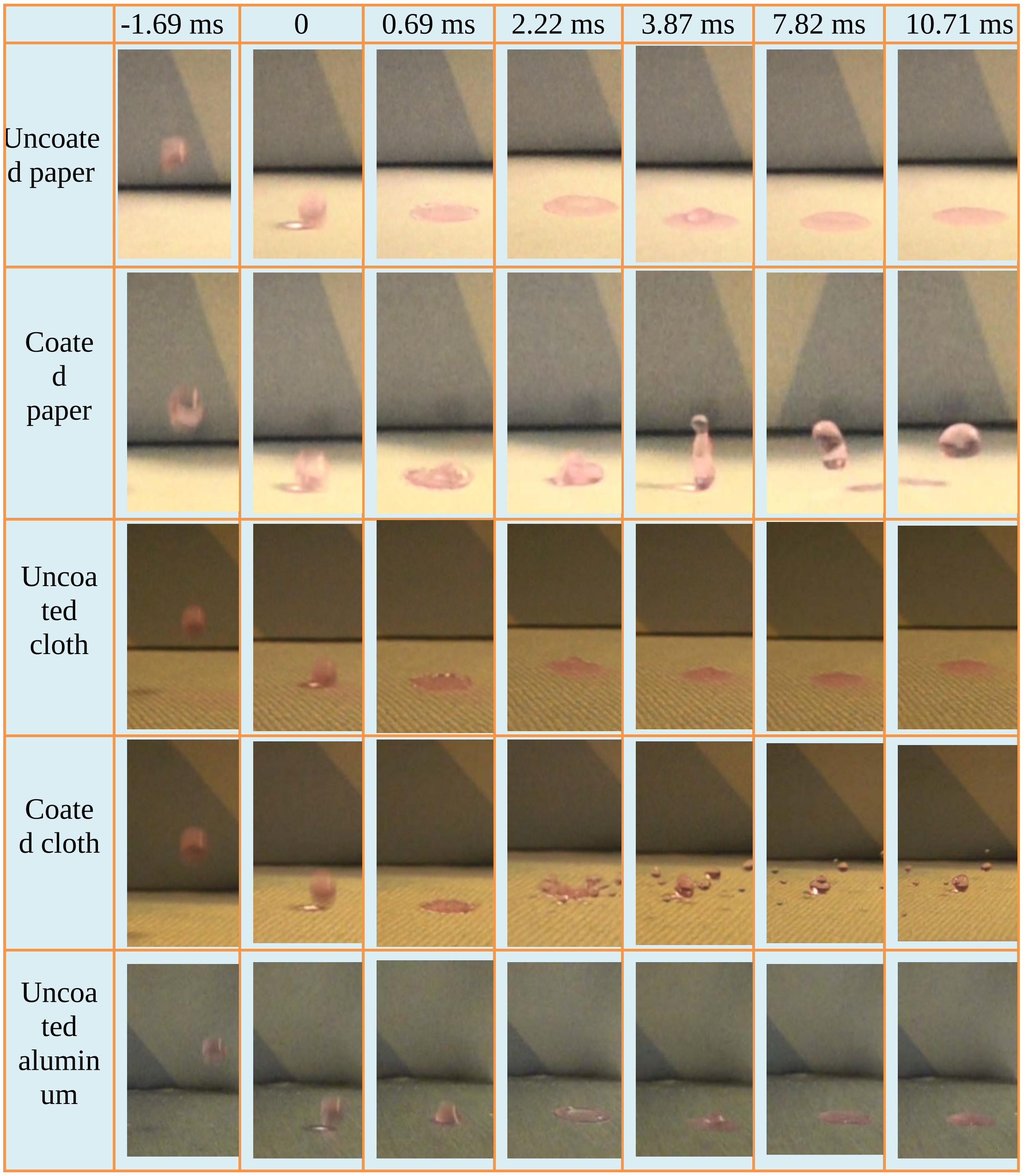

| | | | | | | | |
|---|---|---|---|---|---|---|---|
| Coated aluminum |  |  |  |  | 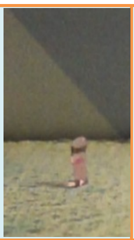 | 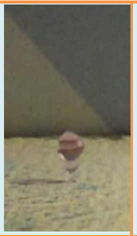 | 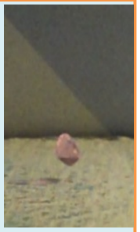 |
| Uncoated glass | 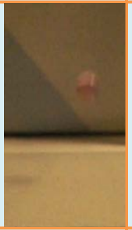 | 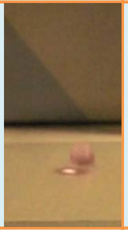 | 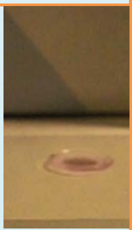 | 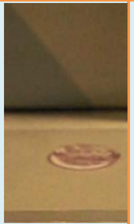 | 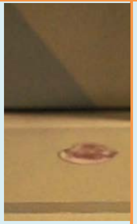 | 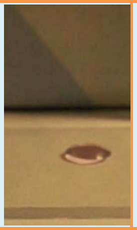 | 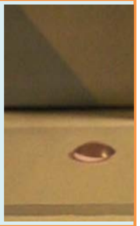 |
| Coated glass |  | 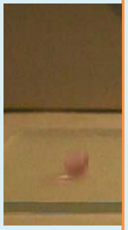 |  | 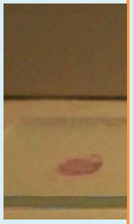 |  | 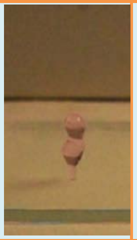 | 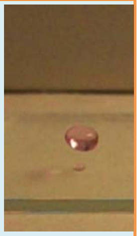 |
| Uncoated acrylic | 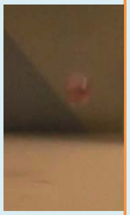 | 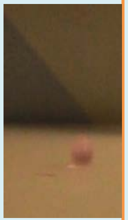 | 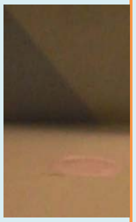 | 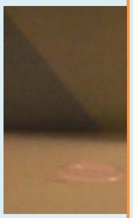 |  |  |  |
| Coated acrylic | 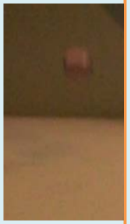 | 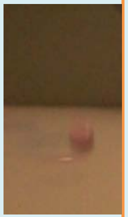 | 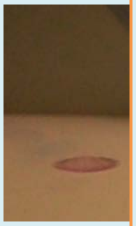 | 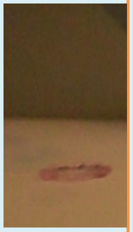 | 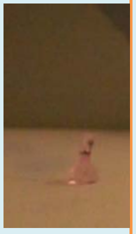 | 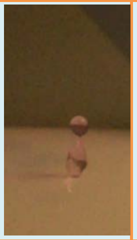 | 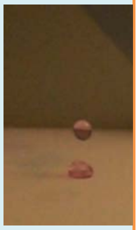 |
| Uncoated steel mesh | 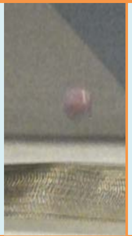 | 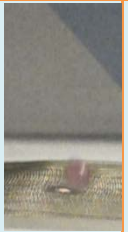 | 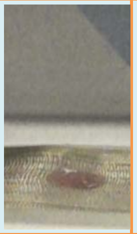 | 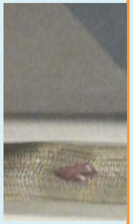 | 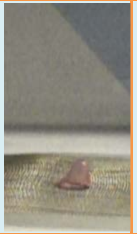 | 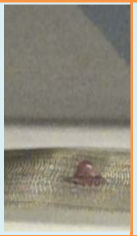 | 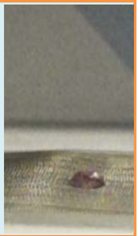 |
| Coated steel mesh |  |  | 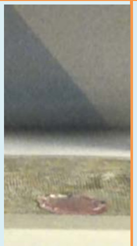 |  |  | 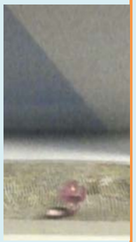 |  |

Figure 45 Time-lapse photographs of water droplets bouncing off coated surfaces and wetting uncoated substrates.

# CHAPTER 5

# CONCLUSIONS AND RECOMMANDATIONS

## 5.1 Conclusions

Superhydrophobic surfaces having very high static water contact angles and low dynamic characteristics were fabricated successfully by spray deposition of two coating solutions on the glass surface. The first layer consists of an epoxy silane GLYMO, that is used as binder/adhesive premier, and the second layer comprises silica nanoparticles surface functionalized by PFOTS. This was achieved following an involved optimization process. The transmittance of the coated surface to the visible light at the wavelength of 400 nm was higher than 70 % and at the wavelength of 800 nm was about 85%. Proper heat treatment by annealing the sample at 300 °C improved the surface transmissivity to visible light by more than 5% at all wavelengths. This is mainly due to the decrease of the surface reflectance caused by the rearrangement of added silica nanoparticles. The produced coating was found to exhibit excellent self-cleaning characteristics as few droplets of water were able to clean a very dusty 25x25 mm surface with an inclination angle of only 10º.

The robustness of the fabricated transparent, superhydrophobic and self-cleaning surfaces was also tested for its resistance to a number of effects expected in outdoor applications. As mentioned above, the coating was found to be thermally stable up to

300°C. The superhydrophobicity of the produced surface remained unaffected after continuous exposure to high intensity UV radiation for about 12 hours. This can be attributed to the high resistance of the functionalized silica films, which are very stable under UV rays.

The surface showed good resistance to pressurized, with no degradation in its superhydrophobicity after having been subjected to a continuous high speed water jet for 1 hour. The coating retained its extreme non-wetting behavior even under the very aggressive abrasion test, performed under 100g weight with abraded against 240 GRIT size sand paper. It took 5 cycles to produce a noticeable degradation of sliding angle and hysteresis.

The unique combination of transparency, water-repellency, mechanical robustness, UV resistance, and thermal stability up to a temperature of 300 °C and excellent self-cleaning properties of the fabricated surfaces make the coating a potential candidate for harsh environment applications.

## 5.2 Recommendations and future work

Based on the results and conclusions of this study, GLYMO used as adhesive layer or binder gave the developed surfaces good mechanical stability and robustness. It was found to be stable under the impact of a water jet, but the surface structure was severely damaged during more aggressive tests of sand blasting.

In the future work, different epoxy silanes having higher hardness and stronger adhesiveness to glass substrate after curing can be investigated as binders to develop more mechanically stable and robust superhydrophobic surfaces. The mechanical stability and robustness of the adhesive layer after its curing are crucial for the abrasion resistance of the developed superhydrophobic surface.

Automatic spray gun is also recommended for use rather than manual spray gun for better and precise control of the film thickness applied on the glass surface. Usage of automatic spray gun may not only result in more uniform and homogenous films, but at the same time allow for good control of deposited silica nanoparticles to ensure superhydrophobicity of surfaces accompanied with high transmittance.

More precise control of the speed of the wind blowing on the superhydrophobic surface and sand particles density traveling together with the wind are also recommended during the sand blasting tests to simulate actual outdoor conditions.

# References

[1] M. A. Green, K. Emery, Y. Hishikawa, W. Warta, and E. D. Dunlop, “Solar cell efficiency tables (Version 45),” *Prog. Photovoltaics Res. Appl.*, vol. 23, no. 1, pp. 1–9, Jan. 2015.

[2] M. A. Green, “The path to 25% silicon solar cell efficiency: History of silicon cell evolution,” *Prog. Photovoltaics Res. Appl.*, vol. 17, no. 3, pp. 183–189, 2009.

[3] A. A. Salim, F. S. Huraib, and N. N. Eugenio, “PV power-study of system options and optimization,” in *EC photovoltaic solar conference. 8*, 1988, pp. 688–692.

[4] F. Wakim, “Introduction of PV power generation to Kuwait,” *Kuwait Inst. Sci. Res. Kuwait City*, 1981.

[5] F. Mejia, J. Kleissl, and J. L. Bosch, “The Effect of Dust on Solar Photovoltaic Systems,” *Energy Procedia*, vol. Complete, no. 49, pp. 2370–2376, 2014.

[6] G. He, C. Zhou, and Z. Li, “Review of Self-Cleaning Method for Solar Cell Array,” *Procedia Eng.*, vol. 16, pp. 640–645, 2011.

[7] R. B. Williams, R. Tanimoto, A. Simonyan, and S. Fuerstenau, “Vibration Characterization of Self-Cleaning Solar Panels with Piezoceramic Actuation,” *48th AIAA/ASME/ASCE/AHS/ASC Struct. Struct. Dyn. Mater. Conf.*, 2007.

[8] P. E. Clark, S. A. Curtis, F. A. Minetto, and J. Keller, “Finding a Dust Mitigation Strategy that Works on the Lunar Surface,” *Lunar Planet. Sci.*, 2007.

[9] C. Callea, C. R. Buh1er ’, J. L. Mcfalib, and S. J. Snyder, “Particle Removal by Electrostatic and Dielectrophoretic Forces for Dust Control During Lunar Exploration Missions,” *J. Electrostat.*, 2009.

[10] A. V. Rao, M. M. Kulkarni, D. P. Amalnerkar, and T. Seth, “Superhydrophobic silica aerogels based on methyltrimethoxysilane precursor,” *J. Non. Cryst. Solids*, vol. 330, no. 1–3, pp. 187–195, 2003.

[11] H. Budunoglu, A. Yildirim, M. O. Guler, and M. Bayindir, “Highly Transparent,

Flexible, and Thermally Stable Superhydrophobic ORMOSIL Aerogel Thin Films," *ACS Appl. Mater. Interfaces*, vol. 3, no. 2, pp. 539–545, Feb. 2011.

[12] S. L. Dhere, S. S. Latthe, C. Kappenstein, G. M. Pajonk, V. Ganesan, A. V. Rao, P. B. Wagh, and S. C. Gupta, "Transparent water repellent silica films by sol-gel process," *Appl. Surf. Sci.*, vol. 256, no. 11, pp. 3624–3629, 2010.

[13] Q. Feng, J. N. Wang, and K. D. Sanderson, "Organic Inorganic Composite," vol. 4, no. 4, pp. 2201–2209, 2010.

[14] S. Liu, X. Liu, S. S. Latthe, L. Gao, S. An, S. S. Yoon, B. Liu, and R. Xing, "Self-cleaning transparent superhydrophobic coatings through simple sol–gel processing of fluoroalkylsilane," *Appl. Surf. Sci.*, vol. 351, pp. 897–903, 2015.

[15] P. G. Parejo, M. Zayat, and D. Levy, "Highly efficient UV-absorbing thin-film coatings for protection of organic materials against photodegradation," *J. Mater. Chem.*, vol. 16, no. 22, p. 2165, 2006.

[16] R. Taurino, E. Fabbri, D. Pospiech, A. Synytska, and M. Messori, "Preparation of scratch resistant superhydrophobic hybrid coatings by sol-gel process," *Prog. Org. Coatings*, vol. 77, no. 11, pp. 1635–1641, 2014.

[17] Y. Xiu, Y. Liu, B. Balu, D. W. Hess, and C. Wong, "Robust superhydrophobic surfaces prepared with epoxy resin and silica nanoparticles," *IEEE Trans. Components, Packag. Manuf. Technol.*, vol. 2, no. 3, pp. 395–401, 2012.

[18] G. Bracco and B. Holst, *Surface science techniques*, vol. 51, no. 1. 2013.

[19] J. P. Youngblood and T. J. McCarthy, "Ultrahydrophobic polymer surfaces prepared by simultaneous ablation of polypropylene and sputtering of poly(tetrafluoroethylene) using radio frequency plasma," *Am. Chem. Soc. Polym. Prepr. Div. Polym. Chem.*, vol. 40, no. 2, pp. 563–564, 1999.

[20] E. Wolfram, R. Faust, and J. Padday, "Wetting, spreading and adhesion," *JF Padday, Ed*, 1978.

[21] A. W. Neumann, "Contact angles and their temperature dependence:

thermodynamic status, measurement, interpretation and application," *Adv. Colloid Interface Sci.*, vol. 4, no. 2–3, pp. 105–191, 1974.

[22] A. Cassie, "40, 546 (1944): S. Baxter, ABD Cassie," *J. Text. Inst*, 1945.

[23] R. N. Wenzel, "Resistance of Solid Surfaces to Wetting by Water," *Ind. Eng. Chem.*, vol. 28, no. 8, pp. 988–994, Aug. 1936.

[24] R. E. Johnson and R. H. Dettre, "Contact Angle Hysteresis. III. Study of an Idealized Heterogeneous Surface," *J. Phys. Chem.*, vol. 68, no. 7, pp. 1744–1750, 1964.

[25] Z. Yoshimitsu, A. Nakajima, T. Watanabe, and K. Hashimoto, "Effects of surface structure on the hydrophobicity and sliding behavior of water droplets," *Langmuir*, vol. 18, no. 15, pp. 5818–5822, 2002.

[26] D. Öner and T. J. McCarthy, "Ultrahydrophobic surfaces. Effects of topography length scales on wettability," *Langmuir*, vol. 16, no. 20, pp. 7777–7782, 2000.

[27] R. D. Hazlett, "Fractal applications: Wettability and contact angle," *J. Colloid Interface Sci.*, vol. 137, no. 2, pp. 527–533, 1990.

[28] S. Shibuichi, T. Onda, N. Satoh, and K. Tsujii, "Super Water-Repellent Surfaces Resulting from Fractal Structure," *J. Phys. Chem.*, vol. 100, no. 50, pp. 19512–19517, Jan. 1996.

[29] A. Nakajima, A. Fujishima, K. Hashimoto, and T. Watanabe, "Preparation of Transparent Superhydrophobic Boehmite and Silica Films by Sublimation of Aluminum Acetylacetonate," *Adv. Mater.*, vol. 11, no. 16, pp. 1365–1368, Nov. 1999.

[30] Hideo Nakae, Ryuichi Inui, Yosuke Hirata, and Hiroyuki Saito, "Effects of surface roughness on wettability," *Acta Mater.*, vol. 46, no. 7, pp. 2313–2318, 1998.

[31] H. Budunoglu, "Higly transparent, flexible, and thermal stable superhydrophobic ORMOSIL aerogel thin films," *Appl. Mater. Interfaces*, pp. 539–545, 2010.

[32] N. Gao, Y. Y. Yan, X. Y. Chen, and D. J. Mee, "Superhydrophobic surfaces with

hierarchical structure," *Mater. Lett.*, vol. 65, no. 19–20, pp. 2902–2905, 2011.

[33] M. Jin, X. Feng, J. Xi, J. Zhai, K. Cho, L. Feng, and L. Jiang, "Super-Hydrophobic PDMS Surface with Ultra-Low Adhesive Force a," pp. 1805–1809, 2005.

[34] T. Young, "An Essay on the Cohesion of Fluids," *Philos. Trans. R. Soc. London*, vol. 95, no. 0, pp. 65–87, 1805.

[35] G. H. Findenegg and S. Herminghaus, "Wetting: Statics and dynamics," *Curr. Opin. Colloid Interface Sci.*, vol. 2, no. 3, pp. 301–307, 1997.

[36] T. Jesionowski, J. Zurawska, and A. Krysztafkiewicz, "Surface properties and dispersion behaviour of precipitated silicas," *J. Mater. Sci.*, vol. 37, no. 8, pp. 1621–1633, 2002.

[37] P. Buisson, C. Hernandez, M. Pierre, and A. . Pierre, "Encapsulation of lipases in aerogels," *J. Non. Cryst. Solids*, vol. 285, no. 1–3, pp. 295–302, Jun. 2001.

[38] A. Venkateswara Rao and D. Haranath, "Effect of methyltrimethoxysilane as a synthesis component on the hydrophobicity and some physical properties of silica aerogels," *Microporous Mesoporous Mater.*, vol. 30, no. 2–3, pp. 267–273, 1999.

[39] R. Ciriminna, A. Fidalgo, V. Pandarus, L. M. Ilharco, M. Pagliaro, and A. R. Pais, "The Sol − Gel Route to Advanced Silica-Based Materials and Recent Applications," 2012.

[40] M. S. Lee and N. J. Jo, "Coating of Methyltriethoxysilane—Modified Colloidal Silica on Polymer Substrates for Abrasion Resistance," *J. Sol-Gel Sci. Technol.*, vol. 24, no. 2, pp. 175–180, 2002.

[41] L. Y. L. Wu, E. Chwa, Z. Chen, and X. T. Zeng, "A study towards improving mechanical properties of sol-gel coatings for polycarbonate," *Thin Solid Films*, vol. 516, no. 6, pp. 1056–1062, 2008.

[42] A. Venkateswara Rao, S. S. Latthe, D. Y. Nadargi, H. Hirashima, and V. Ganesan, "Preparation of MTMS based transparent superhydrophobic silica films by sol-gel method," *J. Colloid Interface Sci.*, vol. 332, no. 2, pp. 484–490, 2009.

[43] M. Psarski, J. Marczak, G. Celichowski, G. B. Sobieraj, K. Gumowski, F. Zhou, W. Liu, and V. sp oo, “Hydrophobization of epoxy nanocomposite surface with 1H,1H,2H,2H-perfluorooctyltrichlorosilane for superhydrophobic properties,” *Cent. Eur. J. Phys.*, vol. 10, no. 5, pp. 1197–1201, 2012.

[44] Takashi Nishino, Masashi Meguro, Katsuhiko Nakamae, A. Motonori Matsushita, and Y. Ueda, “The Lowest Surface Free Energy Based on −CF3 Alignment,” 1999.

[45] E. F. Hare, E. G. Shafrin, and W. A. Zisman, “Properties of films of adsorbed fluorinated acids,” *J. Phys. Chem.*, vol. 58, no. 3, pp. 236–239, 1954.

[46] E. Lindner and E. Arias, “Surface free energy characteristics of polyfluorinated silane films,” *Langmuir*, vol. 8, no. 4, pp. 1195–1198, Apr. 1992.

[47] B. Bhushan, Y. C. Jung, and K. Koch, “Micro-, nano- and hierarchical structures for superhydrophobicity, self-cleaning and low adhesion,” *Philos. Trans. R. Soc. London A Math. Phys. Eng. Sci.*, vol. 367, no. 1894, 2009.

[48] D. Byun, J. Hong, and Saputra, “Wetting Characteristics of Insect Wing Surfaces,” *J. Bionic Eng.*, vol. 6, no. 1, pp. 63–70, Mar. 2009.

[49] Y. Yoon, D. Kim, and J.-B. Lee, “Hierarchical micro/nano structures for super-hydrophobic surfaces and super-lyophobic surface against liquid metal,” *Micro Nano Syst. Lett.*, vol. 2, no. 1, p. 3, Dec. 2014.

[50] H. Zhang, Y. Ma, J. Tan, X. Fan, Y. Liu, J. Gu, B. Zhang, H. Zhang, and Q. Zhang, “Robust, self-healing, superhydrophobic coatings highlighted by a novel branched thiol-ene fluorinated siloxane nanocomposites,” *Compos. Sci. Technol.*, vol. 137, pp. 78–86, 2016.

[51] K. S. S. Kumar, V. Kumar, and C. P. R. Nair, “Bulk superhydrophobic materials: a facile and efficient approach to access superhydrophobicity by silane and urethane chemistries,” *J. Mater. Chem. A*, vol. 2, no. 37, p. 15502, Jul. 2014.

[52] D. Bersani, P. . Lottici, M. Casalboni, and P. Prosposito, “Structural changes induced by the catalyst in hybrid sol–gel films: a micro-Raman investigation,”

2001.

[53] J. Mihály, S. Sterkel, H. M. Ortner, L. Kocsis, L. Hajba, É. Furdyga, and J. Mink, “FTIR and FT-Raman Spectroscopic Study on Polymer Based High Pressure Digestion Vessels,” *Croat. Chem. Acta*, vol. 79, no. 3, pp. 497–501, 2006.

[54] S. Herminghaus, “Roughness-induced non-wetting,” *Europhys. Lett.*, vol. 79, no. 5, p. 59901, Sep. 2007.

[55] M. Nosonovsky, B. Bhushan, A. A. V, and A, “Roughness-induced superhydrophobicity: a way to design non-adhesive surfaces,” *J. Phys. Condens. Matter*, vol. 20, no. 22, p. 225009, Jun. 2008.

[56] Q. Zheng and C. Lü, “Size Effects of Surface Roughness to Superhydrophobicity,” *Procedia IUTAM*, vol. 10, pp. 462–475, 2014.

[57] G. Hassan, B. S. Yilbas, S. A. M. Said, N. Al-Aqeeli, and A. Matin, “Chemo-Mechanical Characteristics of Mud Formed from Environmental Dust Particles in Humid Ambient Air.,” *Sci. Rep.*, vol. 6, p. 30253, Jul. 2016.

[58] L. Xu, D. Zhu, X. Lu, and Q. Lu, “Transparent, Thermally and Mechanically Stable Superhydrophobic Coating Prepared by Electrochemical Template strategy,” *J. Mater. Chem. A*, 2015.

[59] M. . Alam and D. . Cameron, “Optical and electrical properties of transparent conductive ITO thin films deposited by sol–gel process,” *Thin Solid Films*, vol. 377, pp. 455–459, 2000.

[60] S.-S. Kim, S.-Y. Choi, C.-G. Park, and H.-W. Jin, “Transparent conductive ITO thin films through the sol-gel process using metal salts,” *Thin Solid Films*, vol. 347, no. 1, pp. 155–160, 1999.

[61] Y. Xiu, D. W. Hess, and C. P. Wong, “UV and thermally stable superhydrophobic coatings from sol–gel processing,” *J. Colloid Interface Sci.*, vol. 326, no. 2, pp. 465–470, 2008.

[62] L. M. Johnson, L. Gao, C. Shields IV, M. Smith, K. Efimenko, K. Cushing, J.

Genzer, and G. P. López, “Elastomeric microparticles for acoustic mediated bioseparations,” *J. Nanobiotechnology*, vol. 11, no. 1, p. 22, Jun. 2013.

[63] H. Wang, J. Fang, T. Cheng, J. Ding, L. Qu, L. Dai, X. Wang, and T. Lin, “One-step coating of fluoro-containing silicananoparticles for universal generation of surface superhydrophobicity,” *Chem. Commun.*, vol. 28, no. 7, pp. 877–879, 2008.

[64] K. Nozawa, H. Gailhanou, L. Raison, P. Panizza, H. Ushiki, E. Sellier, J. P. Delville, and M. H. Delville, “Smart Control of Monodisperse Sto 1 ber Silica Particles: Effect of Reactant Addition Rate on Growth Process,” *Langmuir*, vol. 21, pp. 1516–1523, 2005.

[65] P. Wang, J. Liu, W. Chang, X. Fan, C. Li, and Y. Shi, “A facile cost-effective method for preparing robust self-cleaning transparent superhydrophobic coating,” *Appl. Phys. A*, 2016.

[66] S. S. Latthe, H. Imai, V. Ganesan, and A. V. Rao, “Superhydrophobic silica films by sol–gel co-precursor method,” *Appl. Surf. Sci.*, vol. 256, no. 1, pp. 217–222, 2009.

[67] A. Hozumi and O. Takai, “Effect of hydrolysis groups in fluoro-alkyl silanes on water repellency of transparent two-layer hard-coatings,” *Appl. Surf. Sci.*, vol. 103, no. 4, pp. 431–441, 1996.

[68] H. Ni, X. Wang, W. Zhang, X. Wang, and Z. Shen, “Stable hydrophobic surfaces created by self-assembly of poly(methyl methacrylate) end-capped with 2-perfluorooctylethyl methacrylate units,” *Surf. Sci.*, vol. 601, no. 17, pp. 3632–3639, 2007.

[69] M. Mohandes and S. Rehman, “Global Solar Radiation Maps of Saudi Arabia,” *J. Energy Power Eng.*, vol. 4, no. 1237, pp. 1934–8975, 2010.

# Vitae

Name : Abuduliken Bake

Nationality : China

Date of Birth : 4/5/1990

Email : uyablikim@hotmail.com

Address : Building 813 Room 109, KFUPM

Academic Background :

King Fahd University of Petroleum and Minerals | Dhahran, Saudi Arabia

2014.09 – 2017.01 | Master of Science – Material Science and Engineering

Beijing Technology and Business University | Beijing, China

2009.09 – 2013.07 | Bachelor of Engineering - Polymer Materials and Engineering